Geophys. J. Int. (1997) **130**, 283–302

Crustal structure along the EDGE transect beneath the Kodiak shelf off Alaska derived from OBH seismic refraction data

S. Ye, E. R. Flueh, D. Klaeschen and R. von Huene

GEOMAR, Research Center for Marine Geosciences, Wischhofstrasse 1–3, D-24148 *Kiel, Germany. E-mail: sye@geomar.de*

Accepted 1997 March 14. Received 1997 March 13; in original form 1996 August 5

SUMMARY

Along the EDGE Alaska transect over the Kodiak shelf off Alaska, a deep-crustal seismic refraction experiment was carried out in 1994 using an airgun source with a high shot density and closely spaced ocean-bottom hydrophones (OBHs). These data clearly define a gently dipping plate boundary that gradually increases from 2.5° at the trench to 5° 250 km landwards of the trench beneath the shelf. A landward increase of the velocities in the subducting oceanic crust was found. The sedimentary upper plate beneath the continental slope can be divided into a young Neogene accretionary prism beneath the lower slope, and a more layered structure below the middle and upper slope, where a body with elevated velocities (4.2–5.1 km s^{-1}) in the lower part is interpreted as well-consolidated sediment of possibly late Eocene age, acting as the backstop. Across the inner shelf between Kodiak Island and Kenai Peninsula, near-surface high velocities (> 6.0 km s^{-1}) document a strong uplift (> 10 km) of the Mesozoic and Palaeocene accretionary complex, and furthermore suggest its seaward extension beneath the outer shelf. The most striking feature along the EDGE transect is the thick low-velocity zone (LVZ) that coincides with the arched reflectors in the lower crust beneath the Kodiak Island–Kenai Peninsula axis on the EDGE seismic reflection data. This LVZ is interpreted as indicating underplated low-velocity rocks, which contribute the same volume of new material as the frontal accretion to the continent, the growth of which is rapid, totalling 4200 km^2 across the Kodiak shelf since Eocene times. A calculation of the material balance shows that an underplating of underthrust sediment alone may not account for the huge volume of the underplated low-velocity rocks. We speculate that the underplating of continental fragment, or more likely seamounts or plateau, may be involved in continental growth

Key words: accretionary complex, Alaska, continental evolution, crustal structure, underplating.

INTRODUCTION

The Eastern Aleutian arc–trench system has been studied intensively during the three decades since the great 1964 Alaskan earthquake. The margin is unusually broad, extending more than 300 km from the volcanic arc to the trench axis. It is one of a few margins where the older accretionary history is extensively exposed on land and where crustal growth is still active. Structures of late Cretaceous and early Tertiary age commonly belong to terranes that were incorporated into the southern Alaskan landmass, whereas sediments accreted since the Eocene occupy the outer shelf and the continental slope (e.g. Plafker, Moore & Winkler 1994).

The EDGE seismic reflection transect across this margin, comprising lines 301 and 302 (Fig. 1), was acquired in 1989 using a 4 km, 240 channel streamer and a 126 l (7800 cubic inch) airgun source (Moore *et al.* 1991). On the seismic reflection data along EDGE line 301, the plate boundary, represented by the top of the subducting Pacific oceanic crust, could be traced to more than 30 km depth beneath the inner shelf 250 km landwards of the trench (Moore *et al.* 1991). At the lower-crustal level between Kodiak Island and Kenai Peninsula, pronounced layered reflectors, the so-called 'arched reflectors' first identified by Fisher *et al.* (1983), are more clearly and completely imaged. These layered reflectors were interpreted as the large-scale underplating of possibly Eocene sediment (Byrne 1986; Moore *et al.* 1991). However, more constraints, including velocity information, are needed to support this hypothesis further. Although further processing of the data along EDGE line 302 with pre-stack depth-migration techniques improved the original structural resolution and provided a detailed velocity structure within the upper 3–4 km

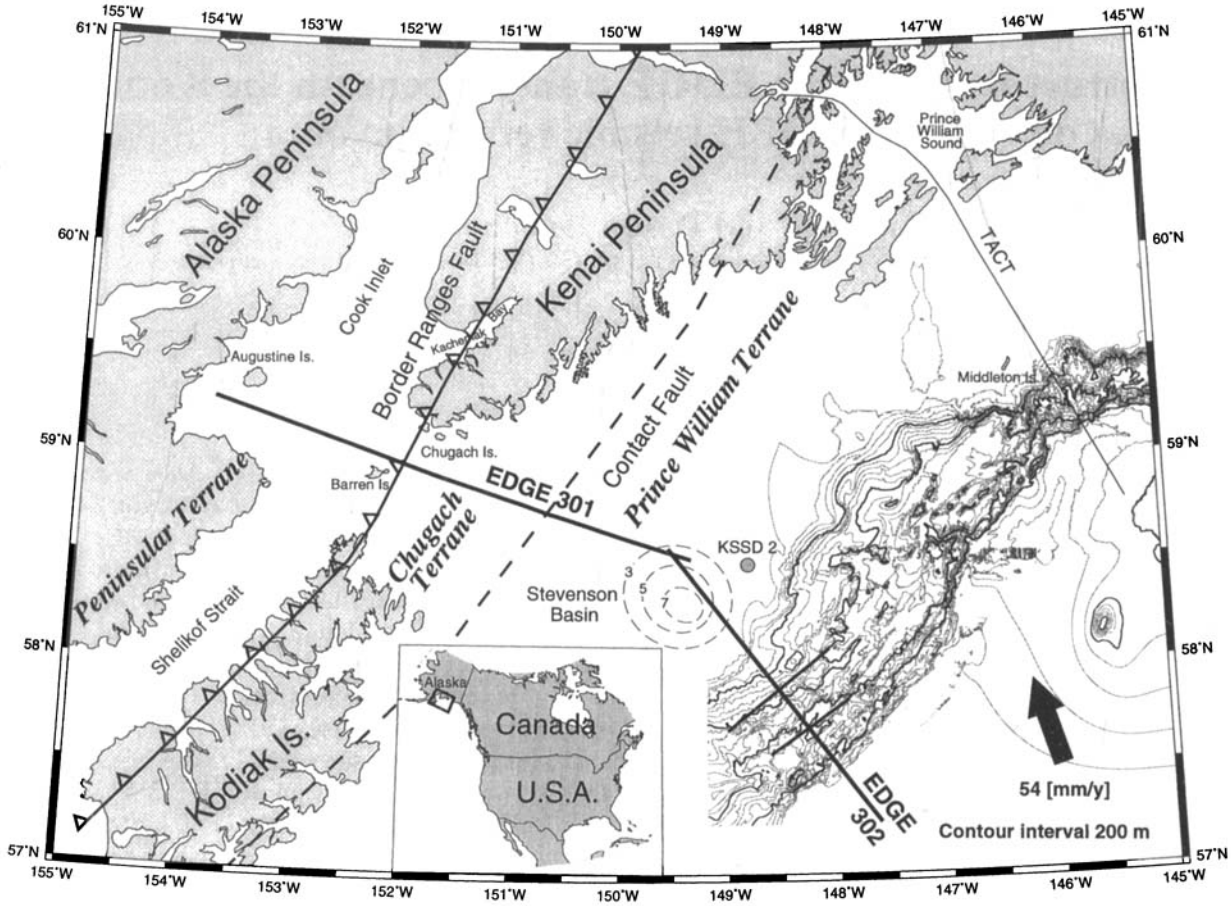

Figure 1. Map of the study area. Bathymetry is drawn from von Huene *et al.* (1997). Thin dashed lines are depth contours in kilometres for the Stevenson Basin.

of the sedimentary sequence (von Huene *et al.* 1997), velocities deeper than a few kilometres below the seafloor were uncertain. A primary objective of this velocity analysis was to estimate the pore fluid loss during accretion and subduction of the thick sediment section.

A wide-angle OBH seismic survey was conducted along the EDGE seismic reflection transect in 1994. The seismic experiment had three objectives:

(1) to image deep crustal structure beyond depths previously observed, including the oceanic crust, the velocity variation within it during the subduction, and the arched reflectors beneath the inner shelf;

(2) to provide velocity information for the improved image reconstruction of the seismic reflection data;

(3) to verify the detailed velocity structure obtained by the pre-stack depth-migration techniques and to provide the missing velocity information for the estimation of the pore fluid loss.

The last objective required high-density wide-angle data using closely spaced OBHs (Fig. 2). In addition to the OBH seismic experiment the area was swath-mapped (Hydrosweep) and active vents were located with deep towed instruments. Water from the vents was sampled and chemically analysed (Suess 1994). Here we present the first results from these seismic data focusing principally on the velocity structure.

TECTONIC SETTING

Along the eastern Aleutian trench the Pacific and North American plates converge at 54 mm a^{-1} in a N15°W direction (DeMets *et al.* 1990) (Fig. 1). The Pacific plate displays Eocene magnetic anomalies at the northeastern end of the Aleutian Trench, which increase in age to the southwest (Griscom & Sauer 1990). The convergent plate geometry was similar throughout much of the Cenozoic (von Huene, Fisher & Bruns 1987; Plafker *et al.* 1994). As the Pacific plate moved northwest along the North American margin into the Gulf of Alaska, it received considerable amounts of sediment, and deep-sea fans were formed. In the study area, the Surveyor Fan has accumulated since 10 Ma and it locally reaches a thickness of more than 3 km at the eastern end of the Aleutian trench (Stevenson & Embley 1987).

The continental margin crossed by the EDGE transect consists of three major terranes, which increase in age from the southeast to northwest (Jones 1982; Plafker, Nokleberg & Lull 1989; Plafker *et al.* 1994). These are the Prince William, the Chugach and the Peninsular terranes, separated by the Contact and Border Ranges fault (BRF) systems (Fig. 1).

The Prince William terrane comprises the continental slope and the adjacent outer shelf. Reflection data show a fundamental break in structure at the middle slope Fig. 3; *cf.* von Huene *et al.* 1997). Seawards of this break lies the recent

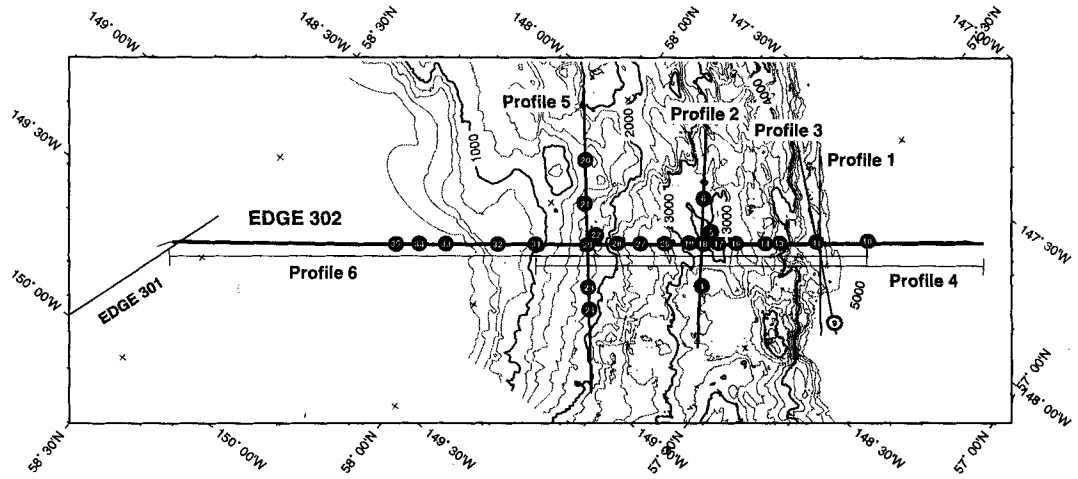

Figure 2. Detailed location map of seismic profiles and OBHs that returned useful data along EDGE 302. Filled (black) circles mark the OBHs used in this study. Thick lines denote the wide-angle seismic profiles presented in this study.

accretionary prism, whereas landwards the contractile structure has a strong landward vergence (Moore *et al.* 1991; von Huene *et al.* 1997). Between these domains is a buttress against which trench sediment was accreted (von Huene *et al.* 1997). It has been inferred from commercial drilling that the upper slope is underlain by Eocene rock (Turner *et al.* 1987).

Beneath the outer shelf is the circular Stevenson forearc basin (von Huene *et al.* 1987), which is floored by Eocene sedimentary rock unconformably overlain by the Neogene sedimentary sequence. This unconformity is commonly marked by discordance and locally by a velocity contrast. However, the density contrast is insufficient to produce the expected negative gravity anomaly (Fisher *et al.* 1983). Eocene turbidite sequences are exposed along the southern side of Kodiak Island (Sitkalidak Formation) and Kenai Peninsula (Valdez and Orca groups); they are juxtaposed further north against Palaeocene volcanic rocks and turbidites that are bordered by the Contact Fault to the north (e.g. Byrne 1986; Plafker *et al.* 1989, 1994).

The Chugach terrane is a narrow belt of the Mesozoic accretionary complex consisting mainly of deep-sea turbidites that exhibit metamorphism of the prehnite–pumpellyite facies (Sample & Moore 1987). The Mesozoic and Palaeocene accretionary complexes are crossed by earliest Tertiary intrusives (58–60 Ma), which were generated by the subducting Kula–Farallon spreading ridge (Hill, Morris & Whelan 1981; Moore *et al.* 1983). The Eocene complex is penetrated by younger intrusives (53–49 Ma) from possible small ridges of the subducting Kula plate (Barker *et al.* 1992).

Within the Peninsular terrane in Cook Inlet, the Palaeozoic continental basement is overlain by an older forearc basin, which developed during the early Jurassic. The sediment thickness of this basin locally reaches 6–8 km (Fisher & Magoon 1978; Fisher 1980; Moore *et al.* 1991). Sedimentary rocks of this basin are thrust over the Mesozoic accretionary complex along the Border Ranges Fault and exposed along the northwestern coast of Kodiak Island and Kenai Peninsula (e.g. Fisher & von Huene 1984).

Although the subduction along the southern Alaska margin has continued since the early Jurassic, the growth of the Kodiak segment of the continental margin has been dominated by two relatively short episodes of accretion, the first in the late Cretaceous and the second in the early Eocene (Byrne 1986; Byrne & Fisher 1987). Rapid lateral growth of the prism in Eocene–Oligocene times coincided with uplift of the Mesozoic core of the prism. During this lateral growth, maintenance of the critical taper required thickening of the prism, which most likely occurred by the underplating of thick sequences of subducted sedimentary units (Moore *et al.* 1991).

FIELDWORK

During the summer of 1994, the R/V Sonne was the platform for an integrated geophysical/geochemical study to estimate the volume and the chemical composition of fluids venting from the Aleutian margin (Flueh & von Huene 1994; Suess 1994). Along with various other surveys, a wide-angle seismic experiment was conducted along the EDGE seismic reflection line (Moore *et al.* 1991). In addition, two short strike refraction lines (profiles 2 and 5) were successfully recorded over the middle and lower slope to improve the velocity control at depth (Fig. 2).

The seismic source, two BOLT CT800 airguns of 4000 cubic inch total volume, was towed at a depth of 12 m and supplied with an air pressure of 130 bar. To minimize interference from water-wave arrivals of the previous shot, the airguns were fired at 60 s intervals, resulting in an average shot spacing of 90 m. As many as 11 digital OBHs (Flueh & Bialas 1996) were used to record shots along a single line segment. Data passed through an anti-aliasing filter of 50 Hz and were continuously recorded with a sampling rate of 200 Hz. The weather conditions were generally favourable, except during the survey along EDGE 301, when strong wind and swell forced termination of the profile prior to its planned completion.

After recovery, the OBH data were copied and split into single shot records stored as a common receiver gather in SEG-Y format. The data were further processed (deconvolved) to compress the reverberation generated by the large-volume airguns and hence to enhance the temporal resolution. In the following only selected examples of record sections are shown. The complete set of all 33 record sections used in this study was included in the cruise report (Flueh & von Huene 1994).

MODELLING OF THE SEISMIC DATA

Data quality and errors of traveltime picks

The data quality varies strongly: it is generally good for OBHs in deep water and moderate to poor in shallow water. Along EDGE line 302 seismic signals can be traced for a distance of up to 50–60 km on most of the record sections used. Traveltimes were picked interactively on a computer display. First arrivals in the near-offset range (<30 km), including refracted waves in the sedimentary section of the upper plate and refracted waves in the oceanic crust, could be accurately defined with error bars varying from ± 0.03 to ± 0.05 s. At larger offsets the first arrivals, mostly refracted waves from the oceanic crust, can be picked with an error bar of typically ± 0.1 s, sometimes ± 0.2 s in the case of very poor signal-to-noise ratio. Refractions and wide-angle reflections from the top of the oceanic crust are clear and continuous over 10–20 km along the strike-lines, whereas along the EDGE line 302 they become increasingly less clear and continuous at OBHs with increasing distance from the trench axis. Their traveltimes can be picked with error bars varying from ± 0.5 to ± 0.1 s. P_mP reflections from the oceanic Moho were clearly recorded by OBHs deployed over the lower and middle slope. However, their exact onset is difficult to define because of the reverberation of the preceding closely spaced refracted waves from the oceanic crust. The error bars are thus relatively large, from ± 0.1 to ± 0.15 s.

Modelling technique

The high data density (e.g. 17 OBHs along the dip-line EDGE 302) makes conventional interactive trial-and-error 2-D ray-tracing modelling and model optimization labour intensive. On the other hand, this high data density is ideal for fast ray tracing and model optimization. In this study forward modelling using MacRay (Luetgert 1992) and automatic inversion using RayInvr (Zelt & Smith 1992) were both performed. The superior graphical user interface of MacRay permits easy model handling, while the automatic ray tracing and the optional automatic inversion of RayInvr uses the dense data coverage to optimize a model rapidly. The modelling of these data was carried out in four steps:

(1) construction of a starting model using *a priori* information, i.e. structure, tectonic units and velocities of the shallow sedimentary cover from reflection data;

(2) optimizing the model until the calculated traveltimes were roughly similar to the observed ones using MacRay;

(3) refining the model by application of automatic inversion;

(4) fine-tuning the resulting model to correct unreasonable values, i.e. velocity values and depths of interfaces, computed by the automatic inversion.

Steps 3 and 4 were iterated several times until no further improvement was achieved. We informally call this approach 'automatic inversion with human assistance'.

Data interpretation

EDGE line 302 (Fig. 3) has a very complex structure due to the rapid change in water depth and the accreted sediment juxtaposed beneath the middle and lower slope. Due to the complexity of the structure to be modelled, and the wave nature of the seismic signals, the velocity model is likely to be spatially aliased, meaning that we may only obtain a smoothed average velocity model, despite the high density of the data. To reduce the ambiguity in modelling, we started modelling the simpler structure along the strike-lines before investigating the more complex structure along EDGE line 302. Unfortunately, our wide-angle line 1 over the front of the accretionary wedge (Fig. 2) failed to record useful data. The repeated line 3 was only partly successful, since only OBH 9 at the end of profile recorded the complete profile (Fig. 2).

The oceanic crust near the trench was modelled first and its structure became a reference section for modelling the subducted oceanic crust along the other lines. Modelling of the strike-lines yielded the basic velocity structure of the overriding plate. These velocity tie points were then used in the starting model of EDGE line 302. Modelling of the structure beneath the continental shelf along EDGE line 301 is described separately at the end of this section.

Structure of the oceanic crust

The EDGE line 302 reflection profile images a strong reflection with strong lateral coherency 30 km seawards of the trench axis, which is interpreted as the top of the igneous oceanic crust (Moore *et al.* 1991; von Huene *et al.* 1997). The horst and graben structure commonly found in this environment is absent. From this we assumed that the oceanic crust is laterally homogenous. It is therefore well determined from only one unreversed OBH observation. Fig. 4 shows the modelling of the oceanic crust from OBH 10 along EDGE line 302, which

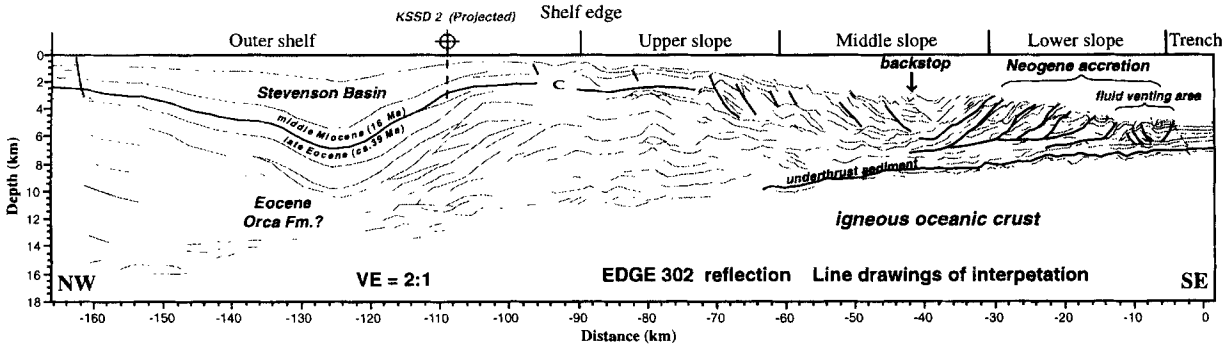

Figure 3. Line drawings of the interpretation of the pre-stack depth-migrated EDGE 302 reflection seismic section (von Huene *et al.* 1997).

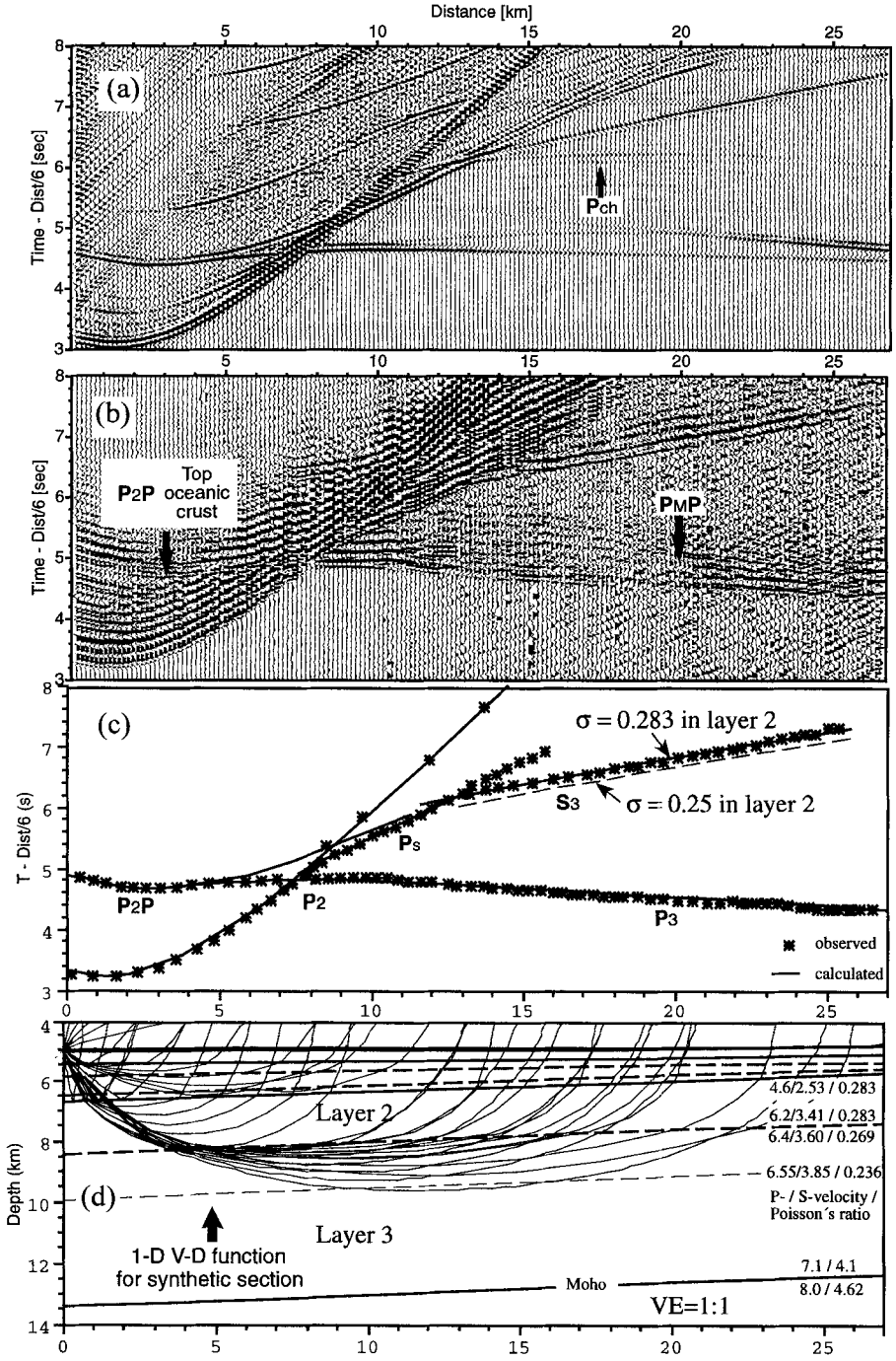

Figure 4. Modelling of seismic data recorded seawards of OBH 10 and the structure of the oceanic crust. (a) Synthetic seismograms using the reflectivity method. The amplitudes are multiplied by the offset to compensate for geometric spreading. The 1-D velocity–depth function corresponds to that at the marked point in the 2-D model in (d). (b) Seismic section of OBH 10 seawards. Each trace represents two seismograms stacked. The amplitude scaling is the same as in (a). (c) Correlated and calculated traveltimes from the 2-D ray-tracing modelling. Dashed line denotes traveltimes if the Poisson's ratio in layer 2 is normal (=0.25). (d) Corresponding ray tracing and the crustal model. Numbers separated by slashes are *P*- and *S*-wave velocities and the Poisson's ratio, respectively.

is located at the trench. The top of the oceanic crust is well imaged on the wide-angle record section (Fig. 4b) as strong near-vertical reflection P_2P (the 2 denotes oceanic layer 2) in the offset range less than 6 km. The corresponding diving waves become first arrivals with a very high amplitude up to 11 km distance, suggesting a strong velocity gradient. Its apparent velocity of close to 6.0 km s^{-1} is seen as diving wave P_2 in layer 2. Beyond 11 km distance a phase turning slightly with an apparent velocity of about 6.5 km s^{-1} is interpreted as refracted waves in layer 3. P_mP is well developed beyond 20 km, although its exact onset is difficult to define. Between the first arrival and water wave lies a diving wave P_s (s denotes sediment) refracted within the sedimentary section.

An unusual feature of this record section is the clear phase

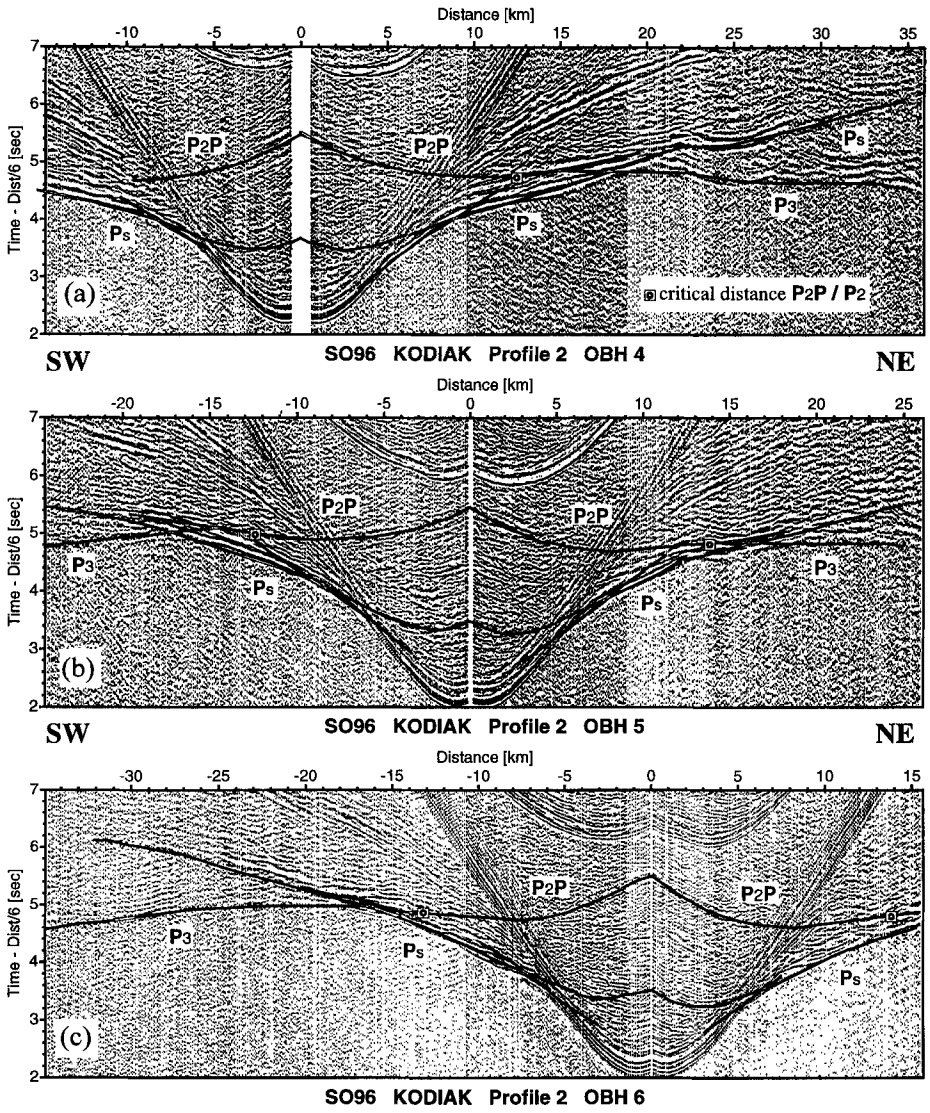

Figure 5. Seismic sections of OBHs 4, 5 and 6 along profile 2 with calculated traveltimes superimposed.

labelled S3, which is interpreted as a converted S wave at the top of the igneous oceanic crust (Fig. 4). Its amplitude is stronger than the primary P waves. Despite the slight dip of the oceanic crust, it is justified to use the reflectivity method to model the amplitude, while the exact traveltime matching required 2-D ray-tracing modelling. Our preferred model with very good fits both in traveltime and amplitude is shown in Fig. 4(d). The top of the oceanic basement was accurately located by matching the traveltime of P_2P (Fig. 4c). A velocity gradient from 4.6 to 6.2 km s^{-1} is needed to match both the traveltimes and the amplitude of refracted wave P_2 in layer 2 up to a distance of 11 km. The synthetic seismic section (Fig. 4a) matches the observations well in amplitude except for the multiple labelled P_{ch}, which channels through the high-gradient layer 2 and is delayed by an S_3-like S wave within the oceanic crust. The lack of a corresponding phase in the observations indicates that our single-layer approximation for layer 2 with a constant velocity gradient is too simple; it probably has a more complex structure (Spudich & Orcutt 1980a). The stronger amplitude of the S_3 wave was successfully modelled by assuming a higher S-wave than P-wave velocity gradient (Fig. 4a). This higher gradient resulted in a decreasing Poisson's ratio with depth in the upper part of layer 3. We want to stress here that the Poisson's ratio determined for layer 2 represents an average value, since it was calculated by changing the Poisson's ratio uniformly in layer 2 in order to fit the traveltimes of S_3.

Profile 2, strike-line

Profile 2 is located 37 km from the trench axis on the lower slope, and was recorded on three OBHs at a water depth of about 3000 m (Fig. 2). Diving waves from the sedimentary section in the overriding plate form the first arrivals P_s from small distances ($\approx$5 km) and are easily traced to distances of up to 30 km (Fig. 5). The secondary phase behind P_s at around 14–19 km distance at $\approx$5 s reduced traveltime, which is especially clear on OBH 4 to the right (NE) (Fig. 5a), is interpreted as P_2P/P_2, i.e. the critical reflection from, and diving waves in, high-gradient oceanic layer 2. The first arrivals beyond 18 km with an apparent velocity over 6.0 km s^{-1} are interpreted as

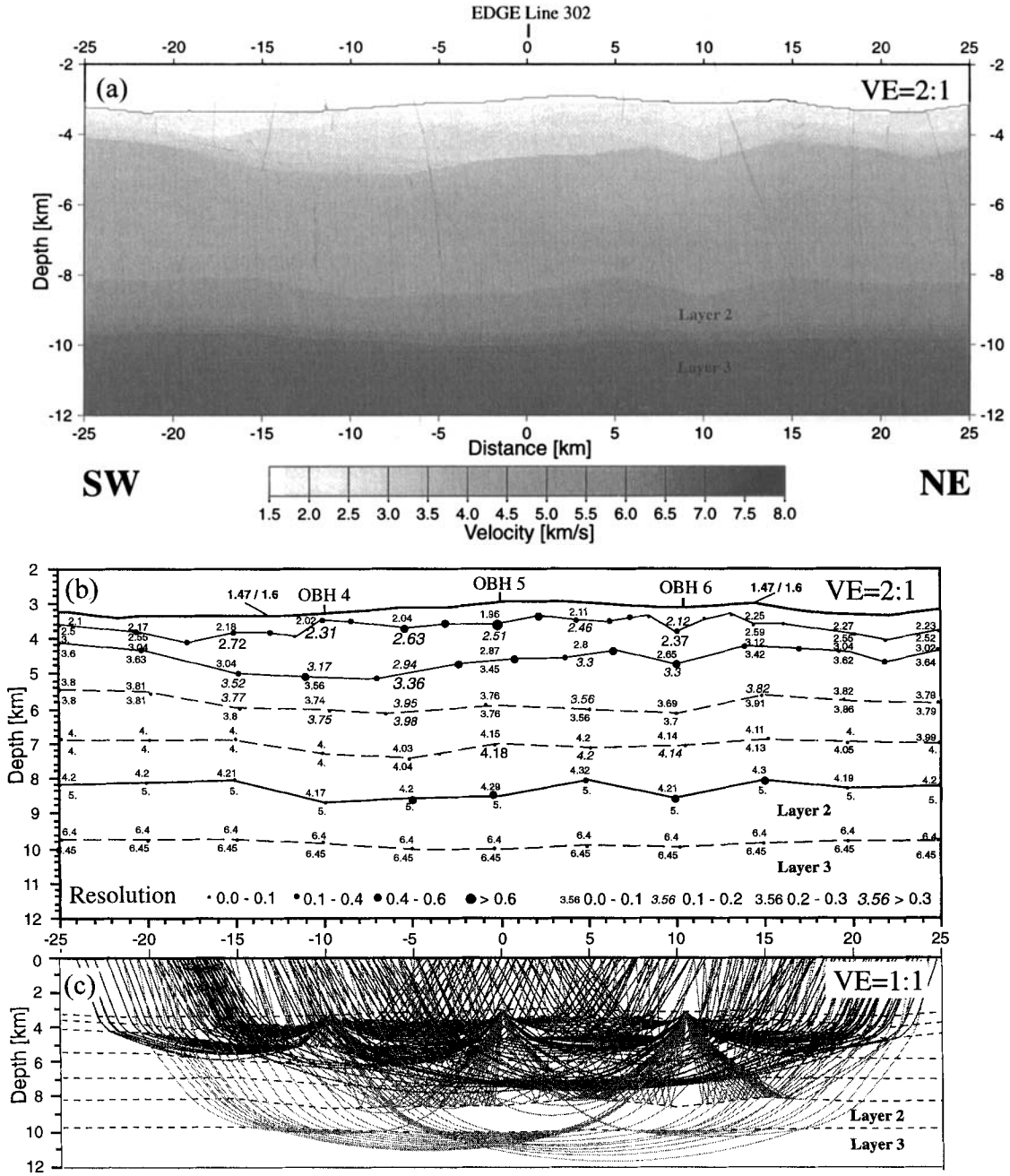

Figure 6. (a) Crustal model of profile 2 with velocities coded in greyscale. (b) Resolution estimates of individual interface and velocity grid points in the crustal model obtained (*cf.* Zelt & Smith 1992). Dashed lines denote interfaces without significant velocity contrast. (c) Ray coverage of the crustal model.

refracted waves P_3 in layer 3 of the subducting oceanic crust. Note the high-amplitude secondary arrivals between 10 and 25 km distance. The multiple of P_s, which was bounced back at the seafloor and travelled within the sedimentary section, is at 5–7 s reduced traveltime. The observation of such a multiple suggests a high positive-downward velocity gradient within the sedimentary section, a possibility thoroughly investigated by Hwang & Mooney (1986).

A close match with the observed traveltimes (Fig. 5) demonstrates the accurate performance of the automatic inversion program RayInvr in layered structures (Fig. 6). The upper plate can be divided essentially into three layers with a moderate velocity contrast between them. A thin layer with a low velocity ($\approx$250 km s^{-1}) at the seafloor is underlain by a layer of laterally varying thickness whose lower boundary has a velocity contrast of about 0.5 km s^{-1}. Velocities then increase to 4.2–4.3 km s^{-1} above oceanic layer 2. A relatively low velocity contrast of 0.8 km s^{-1} along the top of basement (i.e. the top of layer 2) explains the lack of a strong near-vertical reflection from this boundary, in contrast to that observed at OBH 10 near the trench. A velocity of 5.0 km s^{-1} at the top of layer 2 is not required by the traveltime, but by the critical distance of P_2P/P_2, as indicated by the near-zero values of the resolution (Fig. 6b). In accord with subsequent modelling of other lines, a slight

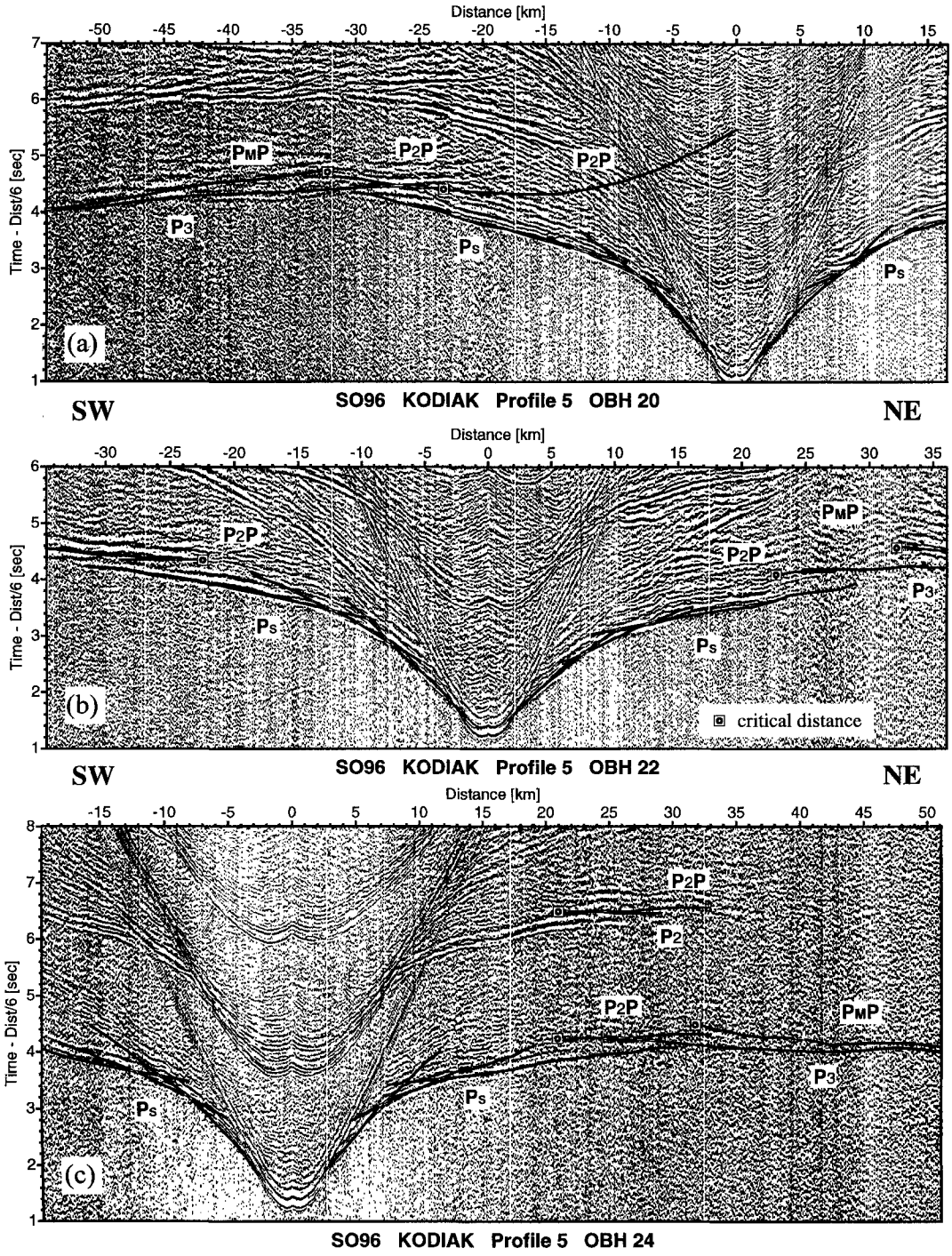

Figure 7. Seismic sections of OBHs 20, 22 and 24 along profile 5 with calculated traveltimes superimposed.

increase of velocity from 6.4 to 6.45 km s^{-1} at the upper boundary of layer 3 was inserted, but it also is not required for the modelling of strike-line 2.

Profile 5, strike-line

Along this 70 km-long line, which crosses the upper slope, five OBHs recorded data of high quality, comparable to line 2. Only three of these record sections (OBHs 20, 22 and 24), with superimposed traveltimes, are shown in Fig. 7. In general they all exhibit characteristics similar to those along profile 2. The cross-over of P_s by P_3 at $\approx$30 km results from the thickening of the sedimentary prism of the upper plate. Phases from the lower plate such as P_2P/P_2 and P_3 are generally strong and clear at OBHs 20 and 21 (not shown here) and on OBH 22 to the SW (to the left in Fig. 7). A P_mP is visible only weakly at the NE end of line. The corresponding velocity model, which matches the observed traveltime well, is shown in Fig. 8. The upper 3–4 km of the overriding plate has a velocity–depth distribution similar to that along profile 2. The discontinuity from 3.0 to 3.5 km s^{-1} at about 1.5 km below the seafloor found in line 2 was also observed here. The velocity increases

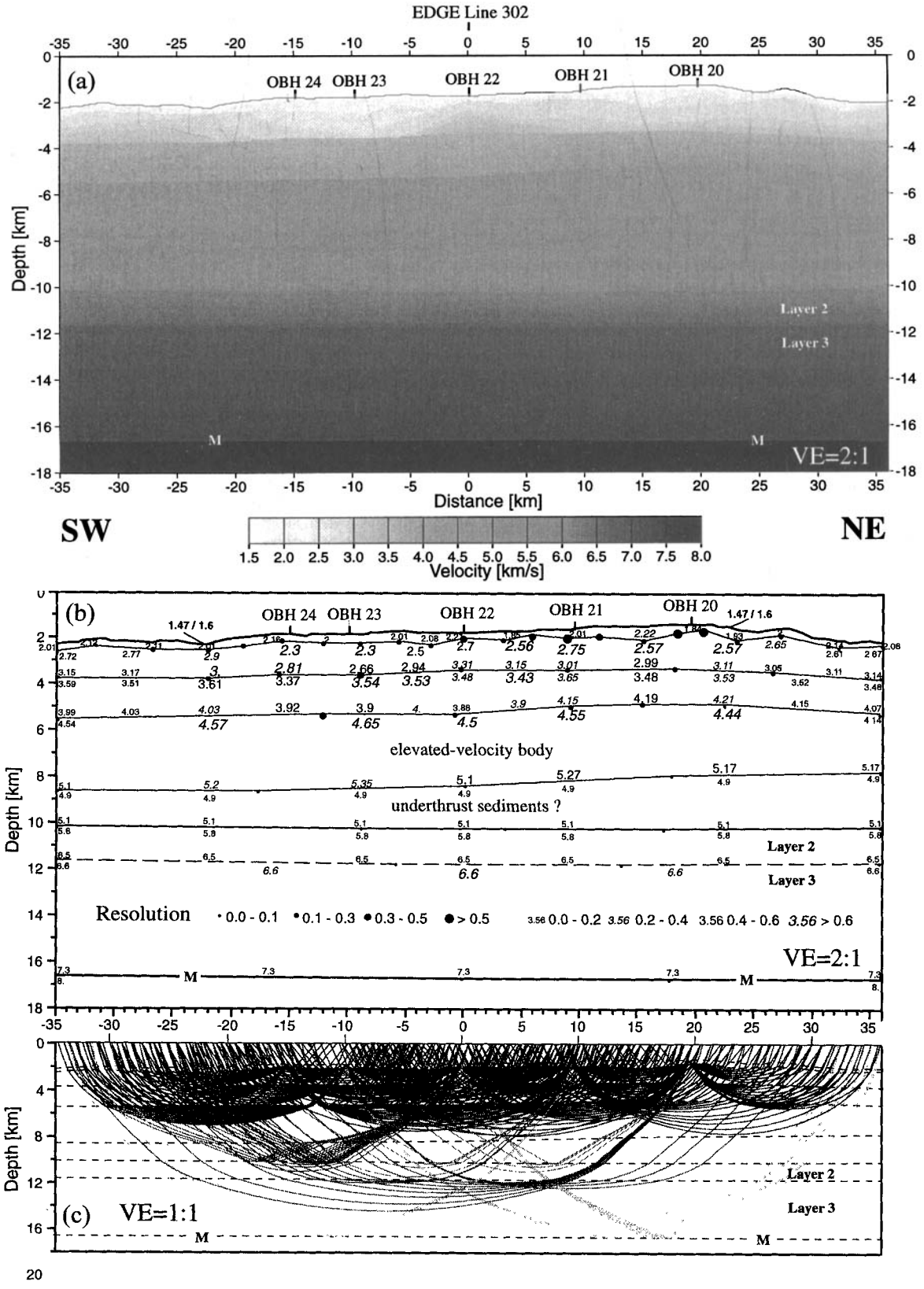

Figure 8. (a) Crustal model of profile 5 with velocities coded in greyscale. (b) Resolution estimates of individual interface and velocity grid points in the crustal model obtained. Dashed line denotes interface without significant velocity contrast. (c) Ray coverage of the crustal model.

gradually to about 4.0 km s^{-1} at 4.5–5.5 km depth, where a second discontinuity is marked by a velocity jump to 4.5–4.6 km s^{-1}. Below that, velocities increase slowly to 5.1 km s^{-1} above the top of a low-velocity zone (LVZ). The top of the oceanic layer 2 lies at 10 km depth. Similar to line 2, a velocity of 5.8 km s^{-1} at the top of layer 2 was not required by the traveltime modelling but was needed to match the critical distance of the P_2P/P_2 When compared with the oceanic crust seawards of the trench axis there is a moderate increase of the velocities to 6.6 km s^{-1} in layer 3. A layer 3 thickness of 5 km fits the weak P_mP reflections observed well, and places the Moho at a depth close to 17 km.

Profiles 4 and 6, EDGE 302

Because of the rapid change in water depth and great lateral variation of structure within the accretionary wedge (Fig. 3), OBHs were deployed at close spacing, some only 3 km apart, to improve spatial resolution. The entire line was shot in two segments with a 76 km-long overlap (Fig. 2). From the 20 OBHs deployed, 17 useful record sections were obtained. Those from the deep-water area were generally high in quality, whereas those from the shelf were of lower data quality. The large number of OBHs and multiple fold of data coverage are appropriate for automatic inversion, but the structure was sufficiently complex to make the inversion unstable. This instability was overcome with a controlled inversion using RayInvr to fix model parameters that were not to be inverted (e.g. water depth and velocity). Optimization of the model was achieved by a stepwise inversion. First we inverted for the shallow structure, then we inverted for the deeper layers of the overriding plate and lastly the oceanic crust, using an approach similar to that described by Zelt & Smith (1992). Following this approach, the match between the observed and calculated traveltimes had misfits of less than 0.05 s for most of the well-defined first arrivals, such as P_s. For later arrivals, P_2P/P_2,

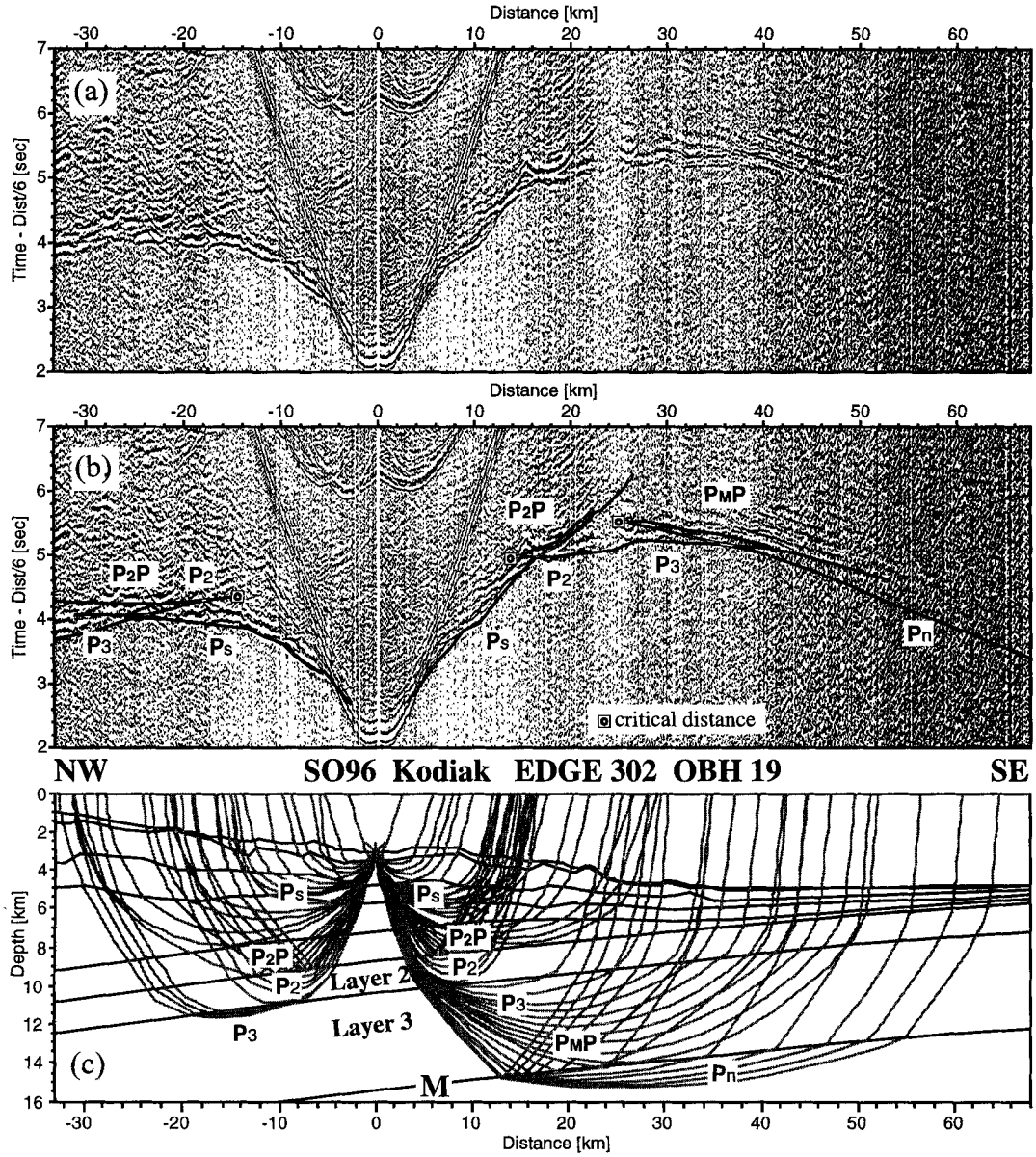

Figure 9. (a) Seismic section of OBH 19; (b) with calculated traveltimes superimposed. (c) Corresponding ray tracing.

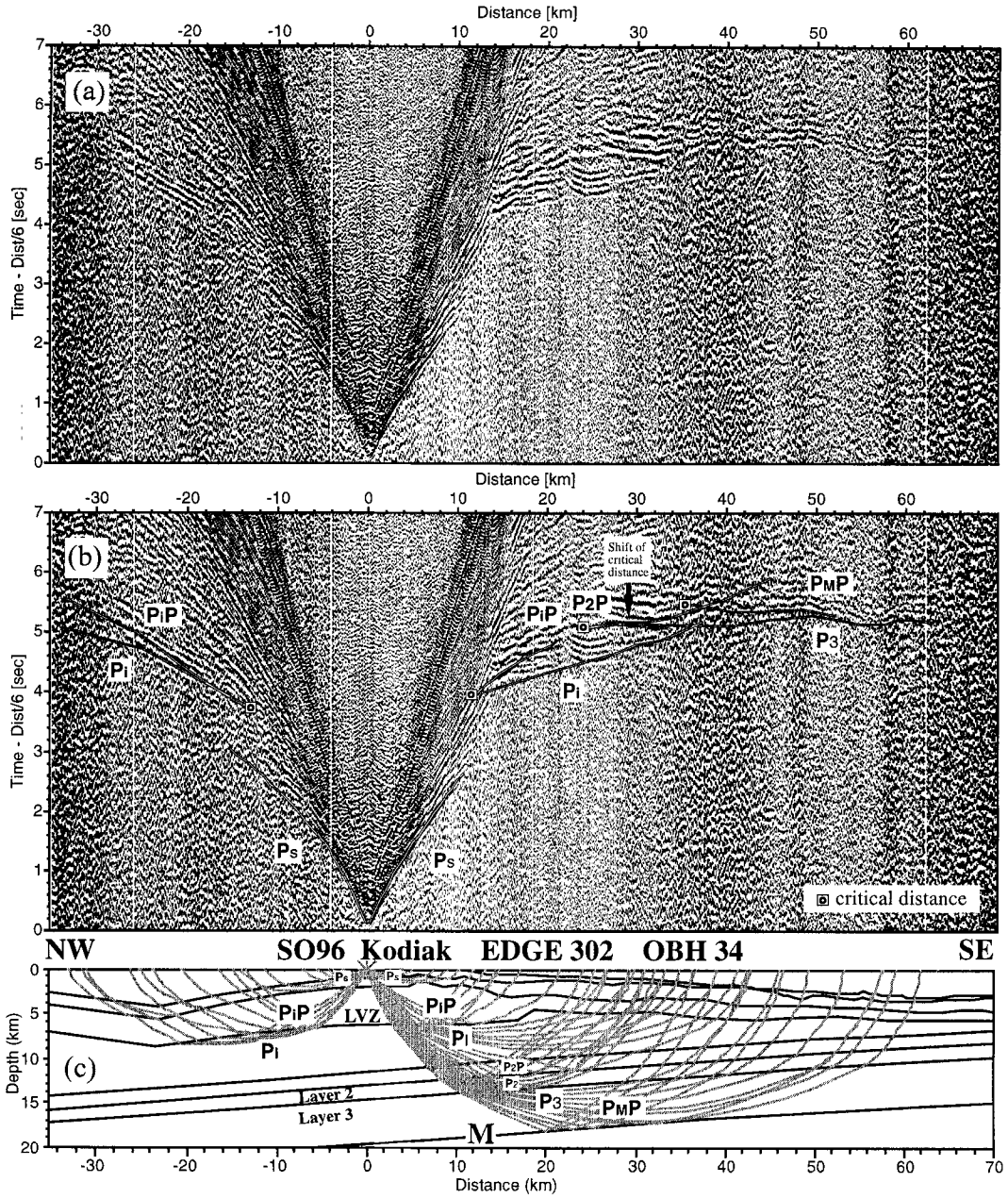

Figure 10. (a) Seismic section of OBH 34; (b) with calculated traveltimes superimposed. Arrow marks the shift of the critical distance of P_2P if the velocity at the top of layer 2 is reduced by 0.3 km s^{-1}. (c) Corresponding ray tracing.

P_mP and P_3, the misfit was close to the traveltime error bar of individual phases (0.1–0.2 s).

Representative record sections recorded over the lower and middle slopes and over the upper slope and shelf illustrate the data quality and traveltime fit (OBHs 19 and 34 in Figs 9 and 10). Data recorded at OBHs across the continental slope show similar characteristics with phase P_s crossed by phase P_3 at various distances. The pronounced asymmetry of traveltime branches mainly reflects the change in water depth. Phase P_2P/P_2 is easily identified at OBHs over the lower slope, but landwards it becomes less clear and disappears under the upper slope. Data recorded at OBHs on the shelf (OBHs 32 to the NW, 33, 34 and 35) reveal an abrupt termination of the phase P_s at around 10 km distance, consistent with a velocity inversion at a shallow depth (Fig. 10). The strong phase labelled P_iP is interpreted as a wide-angle reflection at the base of the velocity inversion. Seaward of OBH 34, phase P_3 can be traced out to a distance of 60 km.

The resulting velocity model is shown in Figs 11 and 12. The velocity field in the subducting plate is rather smooth, increasing gradually landwards from 6.4/7.1 km s^{-1} beneath the trench to 6.6/7.3 km s^{-1} beneath the edge of the shelf, whereas in the accretionary wedge a general downward and landward increase in velocity is observed, marked by pronounced lateral variations. Beneath the middle and upper slope there is a relatively high-velocity body of 4.5–4.6 km s^{-1} 4–5 km below the sea floor. An abrupt change in the structure of the upper plate occurs near the shelf edge. A velocity

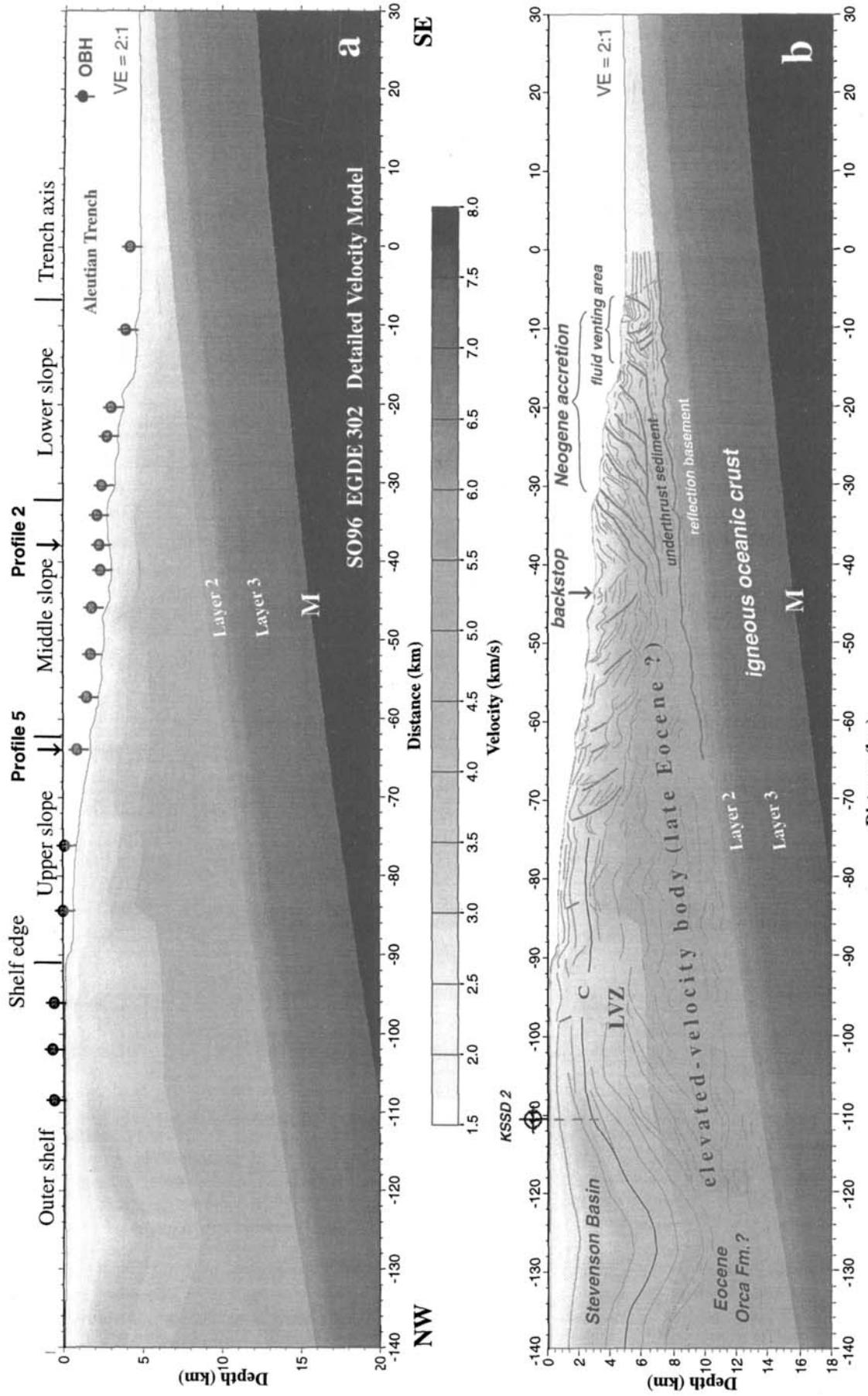

Figure 11. (a) Crustal model of EDGE 302 with velocities coded in grayscale. (b) Superposition with the line drawings of interpretation of the pre-stack depth migrated EDGE 302 reflection seismic section (*cf.* Figure 3)(von Huene *et al.* 1997).

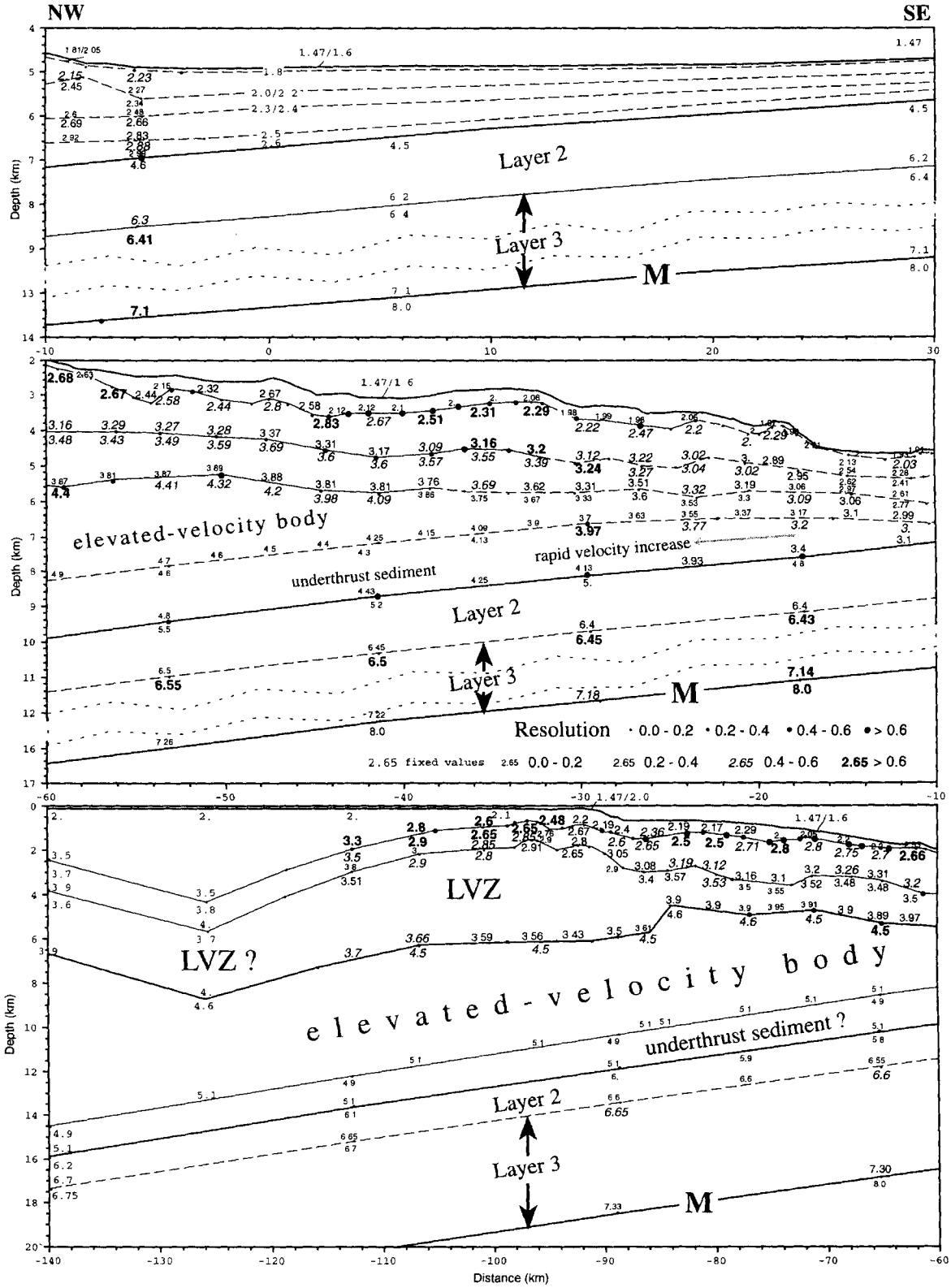

Figure 12. Resolution estimates of individual interface and velocity grid points in the crustal model obtained.

inversion at 2–3 km depth is easily inferred from the termination of the first arrivals P_s of OBHs over the shelf (Fig. 10). The depth of the base of this LVZ and the velocity of the underlying layer are well determined by the critical reflection P_iP and refraction P_i.

DIP LINE EDGE 301

Nine instruments were deployed between the Kenai Peninsula and Kodiak Island (Fig. 13a) to image the arched reflectors observed on reflection data (Fisher *et al.* 1983; Fisher, von

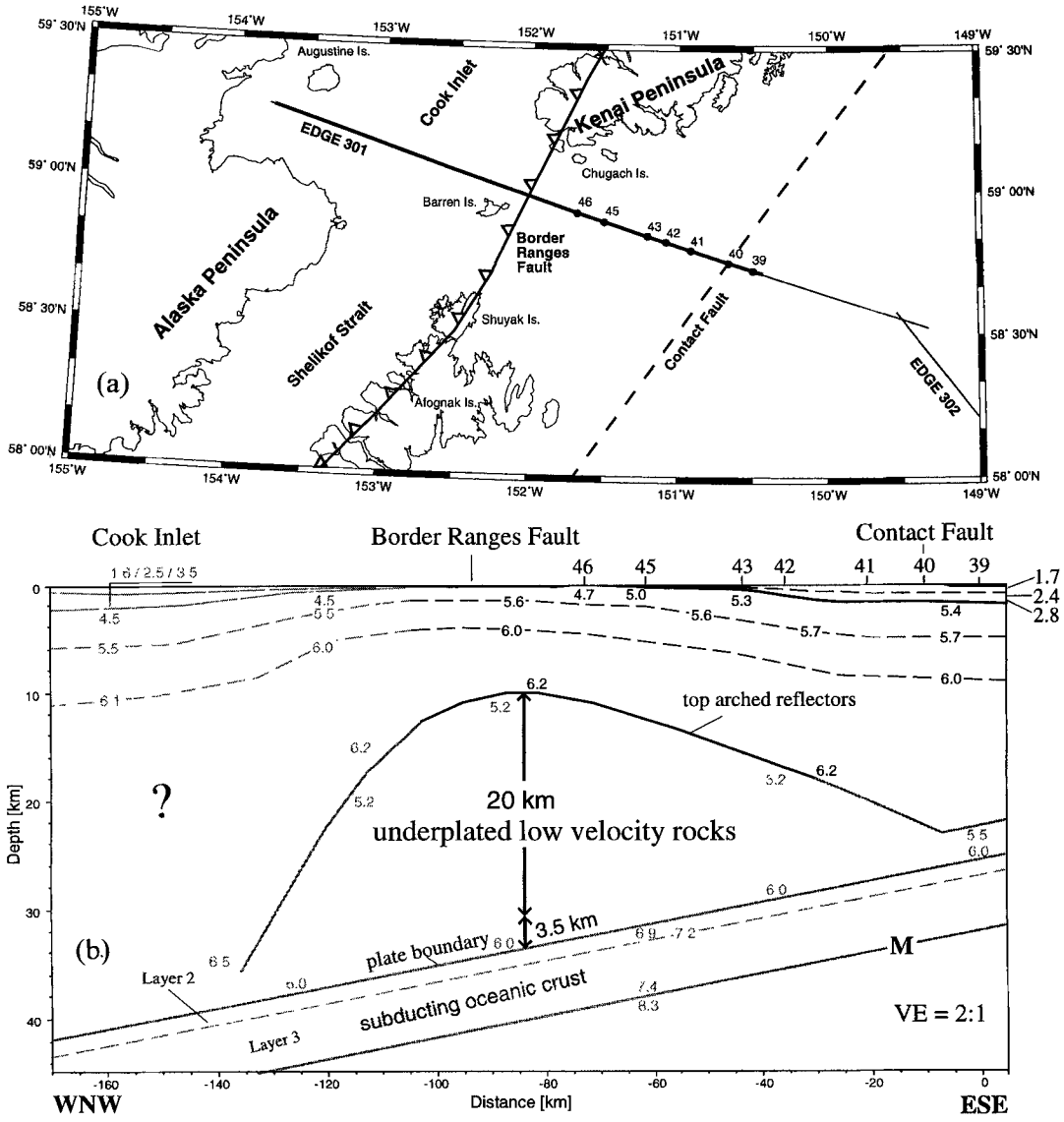

Figure 13. (a) Location map of OBHs along EDGE 301. Thick line denotes the shooting extent of the wide-angle profile. (b) Velocity model beneath the Kodiak shelf. Grey-shaded interfaces and numbers (velocity value in km s^{-1}) are features less well constrained by observation.

Huene & Smith 1987; Moore *et al.* 1991). Airgun shooting began near Augustine volcano, and terminated prematurely near OBH 39 due to the failure of both airguns in rough weather. Although seven instruments returned useful data, the signal-to-noise ratio was rather poor to moderate on most OBHs due to bad weather conditions. Direct waves P_s within the young sediment and refracted waves P_g in the substrata are observed on all record sections. Except for OBH 40 (with a particularly poor signal-to-noise ratio), all record sections display a strong intracrustal reflection P_aP (a denotes arched reflectors) at wide offsets ranging from 20 to 100 km (Fig. 14). In addition, on OBH 39 a strong but discontinuous phase between 80 and 160 km was interpreted as the P_mP reflection.

The structure of the young sedimentary cover and northerly adjacent area is well resolved (Fig. 13b). Velocity increases from 1.7 at the seafloor to 2.8 km s^{-1} at the base at a depth of only 1.8 km, which is characterized by a very high velocity contrast of 2.5 km s^{-1}. Velocities below the young sedimentary cover increase from 5.3–5.4 to 5.6–5.7 km s^{-1} downwards over 2 km and then slowly to 6.2 km s^{-1} immediately above the upper boundary of these arched reflectors, which is well defined by the observed phase P_aP on six OBHs (OBHs 39, 41, 42, 43, 45 and 46). The strong amplitude of P_aP might be interpreted as the overcritical reflection from a high positive velocity contrast. However, in order to explain the Moho reflection P_mP on OBH 39, which has low apparent velocity and time offset relative to the extension of phase P_g in the large offset range, a low-velocity zone (LVZ) is required. A LVZ also better explains the lack of observed refracted waves from below this discontinuity. The velocities of 5.2–6.0 km s^{-1} in the LVZ were chosen to explain the bright reflections from this interface on wide-angle data (Fig. 14). These reflections require a large velocity contrast across the interface. Due to the absence of OBH receivers northwest of OBH 46, the crustal structure northwest of the Border Range Fault is poorly resolved. This

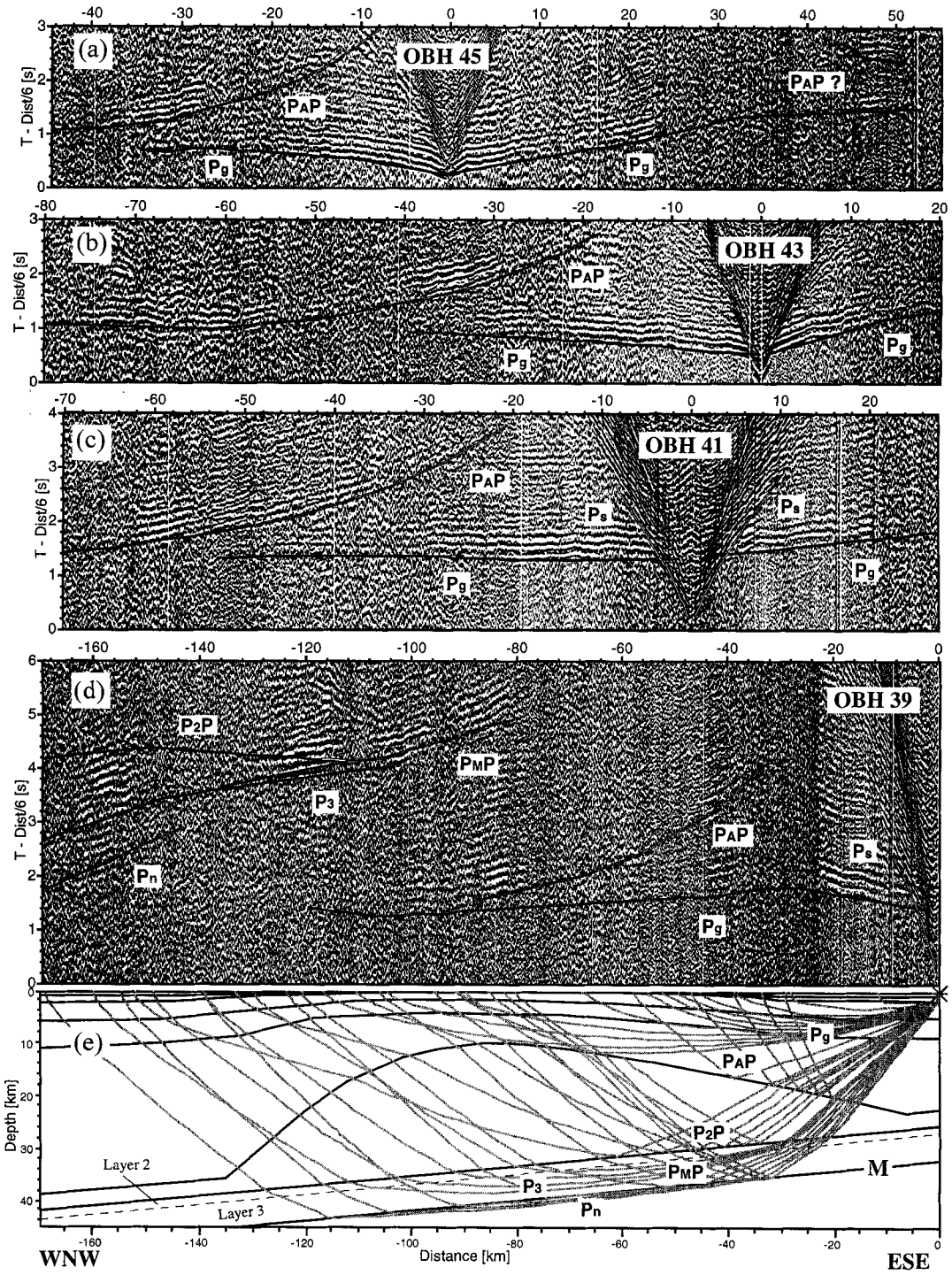

Figure 14. (a)–(d) Seismic sections of OBHs 45, 43, 41 and 39 with calculated traveltimes superimposed. Note that the seismograms were trace-normalized by the rms amplitudes due to the strongly varying noise level. (e) Ray tracing of OBH 39.

lack of resolution may explain the relatively poor match of the P_mP traveltimes for OBH 39 (Fig. 14d). Modelling of P_mP also places a strong constraint on the velocity gradient within the subducting oceanic crust. A low gradient of < 0.25 km s^{-1} in layer 3 was required to match the P_mP and P_3 at large distances. We note that the absence of a P_2P reflection from the plate boundary as arrivals prior to the P_mP reflection is predicted by the arched geometry of the upper boundary of the LVZ, which bounces the P_2P back downwards, even though the plate boundary has a stronger velocity contrast than that at the Moho. Unfortunately, the low signal-to-noise ratio at large offsets on the data at OBHs other than OBH 39 does not permit a correlation of deep crustal phases. We stress here that the crustal structure deeper than the top of the arched reflectors is inadequately resolved and consequently oversimplified.

DISCUSSION

The oceanic crust

The velocity–depth function of the oceanic crust along EDGE 302 is well determined from the newly acquired data, given its 1-D nature. At the trench it is comparable with velocities of Pacific oceanic crust older than 29 Ma compiled by White, McKenzie & O'Nions (1992) and with that derived in the TACT line (Brocher *et al.* 1994) (Fig. 15). The P_n velocity along EDGE 302 is 8.0 km s^{-1}, significantly higher than the 7.7 km s^{-1} determined along the unreversed TACT line. As shown by both the reflection data (Moore *et al.* 1991) and the model derived here, the oceanic crust starts to bend down 30 km before entering the trench, and the dip increases gradually. In contrast, the dip of the converging oceanic crust changes abruptly at the trench from less than 1° to 10° along the TACT line (Brocher *et al.* 1994).

The average Poisson's ratio (0.283) for layer 2 concurs with the common value of 0.28 measured from the rock samples of the ophiolite suite (Salisbury & Christensen 1978; Christensen 1978). This agreement suggests that layer 2 is composed of metabasalt, as proposed for standard oceanic crust (Spudich & Orcutt 1980a,b).

A rapid increase in the P velocity landwards along the top of layer 2 from 4.6 km s^{-1} beneath the trench to 6.1 km s^{-1} beneath the shelf edge (Fig. 15) is not required by the traveltime modelling, as suggested by the low values of the corresponding resolution (Figs 6b, 8b and 12). This is more evident from the observation of the critical distance of the reflection/refraction P_2P/P_2. A 0.3 km s^{-1} variation in the velocity at the top of layer 2 would cause a 5 km shift of the critical distance, large enough to be noticeable in the data (*cf.* Fig 10). This means that even though the critical distance is a semi-quantitative measure, velocities at the top of layer 2 can be determined within an error of $\pm$0.3 km s^{-1}. The rapid increase in the P-velocity landwards along the top of layer 2 is clearly attributed to the reduction in porosity at the top of layer 2, which can be as large as 18 per cent, under increasing overburden pressure (Spudich & Orcutt 1980a). In contrast, the velocity at the top of layer 3 increases only slightly from 6.4 to 6.6 km s^{-1} within the first 100 km landwards of the trench. The velocity at the upper boundary of layer 3 increases further landwards as required by the small velocity gradient in layer 3 to model P_mP on OBH 39 along EDGE 301 (Fig. 14). Below the arched reflectors at a distance of about 250 km landwards of the trench, a velocity of 7.2 km s^{-1} gives the best fit to the observed traveltimes.

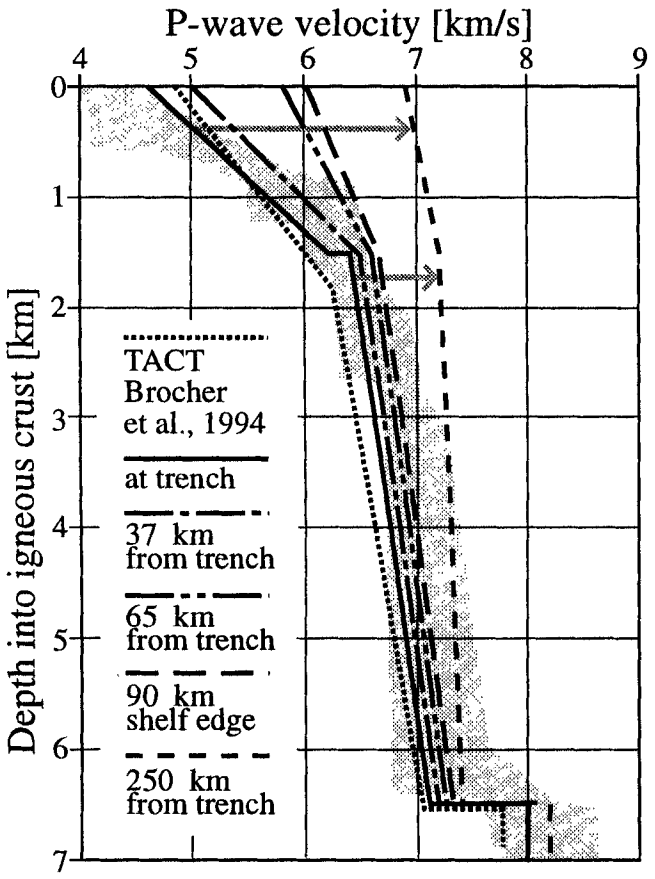

Figure 15. Velocity–depth functions of the oceanic crust at various distances landwards from the trench, illustrating the velocity increase in the oceanic crust during subduction.

Structure of the accretionary wedge along EDGE line 302

The velocity model for the accretionary wedge (Fig. 11a) clearly defines the upper plate as three distinct domains: (1) the seaward domain beneath the lower slope; (2) the landward domain beneath the middle and upper slopes; and (3) the domain beneath the outer shelf between the shelf edge and the Stevenson basin (Fig. 11). In the seaward domain the velocity variation is rather smooth both vertically and landwards, whereas in the landward domain a laterally more homogeneous, well-layered structure with velocity discontinuities roughly parallel to the seafloor shows up clearly. Beneath the shelf edge the structure changes abruptly: a roughly 4 km thick low-velocity zone overlies a discontinuity with velocities from 3.6 to 4.5 km s^{-1} at 6–7 km depth (Fig. 12).

The wide-angle section correlates well with the pre-stack depth-migrated EDGE 302 deep reflection profile (Fig. 11b). The seaward domain corresponds to the Neogene accretionary prism (von Huene *et al.* 1997) with seaward-verging thrust faults, and the landward domain is the zone with landward-verging thrust faults and slope sedimentary cover. The transition between these domains is the location of the backstop. From the complex structure of the imbricate thrust sheets of the Neogene accreted sediment (Figs 3 and 11b), one can infer a complex velocity structure and pronounced lateral inhomogeneity. The smoothed velocity distribution in the seaward half can be explained by the limited lateral resolution of the refraction seismic method, which averages details of the lateral inhomogeneity at the scale of the accretionary structure. The increasing velocity landwards resembles the general trend of the velocity variation expected from the reduction of the porosity by dewatering of the accreted sediment. As illustrated by the strike-lines (Figs 6 and 8) the upper plate exhibits a layered structure. If we consider that the downward gradient of the velocity is mainly caused by compaction, i.e. a reduction of the porosity, the layered structure of the upper plate in the first 3–4 km beneath the seafloor implies that lithostatic pressure controls the sediment compaction process. The 4.0 km s^{-1} and greater velocities in the deep part of the upper plate in the landward domain suggest these deeper substrata are more

consolidated sediment. This consolidation may explain the rigidity required by a backstop to act as a buttress against the accreting sediment. However, the velocity of 4.0–4.3 km s^{-1} at the seaward part of this backstop may suggest this part is not lithified enough to resist the compressional force from the current accretionary prism, and thus is considerably deformed, as suggested by the contractile structure with a strong landward vergence beneath the middle slope.

A decollement overlying a 1.5–2 km thick underthrust sedimentary sequence is imaged in the reflection data (Fig. 3), but remains mostly unresolved in the refraction data (Fig. 11). Beneath the lower slope, the refraction data resolve velocity in the lower part of the upper plate well (Fig. 12). Velocity jumps of less than 0.2 km s^{-1} are insignificant since they are close to the limited resolution. This may imply that the decollement is a thin overpressured zone, as found in the Barbados Ridge (Bangs *et al.* 1990). Velocities in the underthrust sediment increase as gradually as those in the overlying accretionary prism within the first 17 km landwards of the trench axis where the depth of the seafloor changes only slightly (Fig. 12). Further landwards from the steep slope of the seafloor at ~17 model km, velocities in the underthrust sediment increase rapidly from 3.2 to 3.8 km s^{-1} within 6 km (Fig. 12). Our observations contrast with those in the Barbados Ridge complex, where wide-aperture seismic velocities in the underthrust sediment increase slowly (Bangs *et al.* 1990). The rapid velocity increase in the underthrust sediment along EDGE line 302 is in agreement with observations made by Shipley & Moore (1986) and Shipley, Stoffa & Dean (1990) across the Middle American Trench off Costa Rica, where underthrust sediment dewaters within 4 km of the trench axis, resulting in a significant increase in the velocity.

Correlation of reflection and refraction features beneath the outer shelf is difficult (Fig. 11b). The velocity inversion is explained by overpressured pore fluids, which were measured in the nearby borehole KSSD 2 (Turner *et al.* 1987; see Fig. 1 for the location). The top of the LVZ at a depth of around 2 km is comparable with the depth of 1.8 km where the overpressuring occurs (Turner *et al.* 1987). Note that the top of the LVZ does not coincide with horizon C, which is interpreted as the Miocene/Eocene unconformity (von Huene *et al.* 1997). The low velocities between 2.9 and 3.5 km s^{-1} in this LVZ suggest low densities that may be comparable with those of the young sediment infill of the Stevenson basin, and thus explain why no observed gravity anomalies are related to the Stevenson basin, as would be expected from its depth. The largest discrepancy between both sections is the well-imaged reflector, the bottom of the LVZ, at 6–7 km depth in the wide-angle data, which has no counterpart in the reflection section. Since this feature is one of the best-imaged structures on the wide-angle data, derived from the reflection/refraction on OBHs 32–35, an artefact due to a misinterpretation is unlikely. We suspect that the image of this structure is obscured in the reflection data, probably by the complex structure of the reflector itself, which may have a transition zone and/or a rough surface of short wavelength. In the former case the transition zone is thin enough to produce wide-angle reflections but too thick to produce near-vertical reflections. Similarly, the rough surface has a wavelength short enough, if compared with the wavelength of incident wide-angle seismic signals, to produce coherent wide-angle reflections. However, the wavelength of the rough surface is comparable with that of incident near-vertical seismic signals, and no coherent near-vertical reflections can be observed since seismic energy is scattered by the rough surface.

EDGE line 301

The most striking feature here is the huge LVZ with an arched roof centred roughly 10 km beneath the Kodiak Island–Kenai Peninsula axis (Fig. 13). The southeastern slope of this arched roof was well defined by the wide-angle reflections observed on nearly all the OBH data (Fig. 14), and matches the envelope of the arched reflectors (Fig. 16) well. The internal structure of this LVZ, as suggested by the band of arched reflectors (Fig. 16), cannot be resolved by the present wide-angle data and was simplified as a velocity-gradient zone. We wish to stress here that the velocities and thickness of this LVZ cannot be unambiguously determined. Higher overall velocities in this LVZ would lead to a greater thickness and vice versa. The assumed velocities of 5.2–6.0 km s^{-1} in the LVZ should thus be treated cautiously. Nevertheless, the general agreement of the plate boundary between the time-converted model derived from wide-angle seismic data and the reflection data (Fig. 16) suggests that our interpretation of the seismic phases is correct and that the crustal model obtained is reasonable.

Analysis of earthquake and quarry blast records in the seismic array around Kachemak Bay (Fig. 1) in the Kenai Peninsula (Stephens, Page & Lahr 1990) also revealed a prominent reflector, which they named the MUP (Middle Upper Plate) discontinuity, dipping about 20° to the northwest at 13–19 km depth. We propose that this reflector correlates with the northwestern flank of the LVZ observed on EDGE line 301 wide-angle data. Our proposal is further supported by the observation of the *P–S* converted waves at this boundary in the seismological data (Stephens *et al.* 1990), which requires a sharp velocity contrast across this boundary, as found along the EDGE transect.

Rocks with high velocities, from 5.4 to 6.2 km s^{-1}, southeast of the Border Range Fault beneath EDGE line 301 were interpreted as Mesozoic rocks, such as those exposed on Kodiak Island and Kenai Peninsula. The seaward extent of Mesozoic and/or Palaeocene rocks with these velocities is unknown, but they must extend seawards at least to the location of OBH 39 (Fig. 13a). The Contact Fault between the Prince William and Chugach terranes, which lies close to OBH 40, is imaged at depth neither by the reflection data (Moore *et al.* 1991) nor by the wide-angle data.

The elevated velocities of over 5.3 km s^{-1} at the top of the substrata of the young sedimentary cover increase further northwest, reaching as high as 6.0 km s^{-1} at the same depth ($\approx$2 km) vertically over the crest of the LVZ, where the young sedimentary cover also pinches out. These elevated velocities suggest a high degree of lithification related to former burial at a greater depth and document a strong uplift, possibly over 10 km for the Mesozoic accretionary complex in the Kodiak shelf, if we take into account that the comparable velocities of sedimentary rocks were found close to the plate boundary at a depth over 10 km along EDGE line 302 and velocities of $\sim$6.0 km s^{-1} were commonly encountered at a depth of $>$10 km beneath the Chugach and Prince William terranes (Flueh *et al.* 1989; Fuis *et al.* 1991; Brocher *et al.* 1994). This observation agrees well with the surface geological evidence on Kodiak Island and Kenai Peninsula for an uplift of the

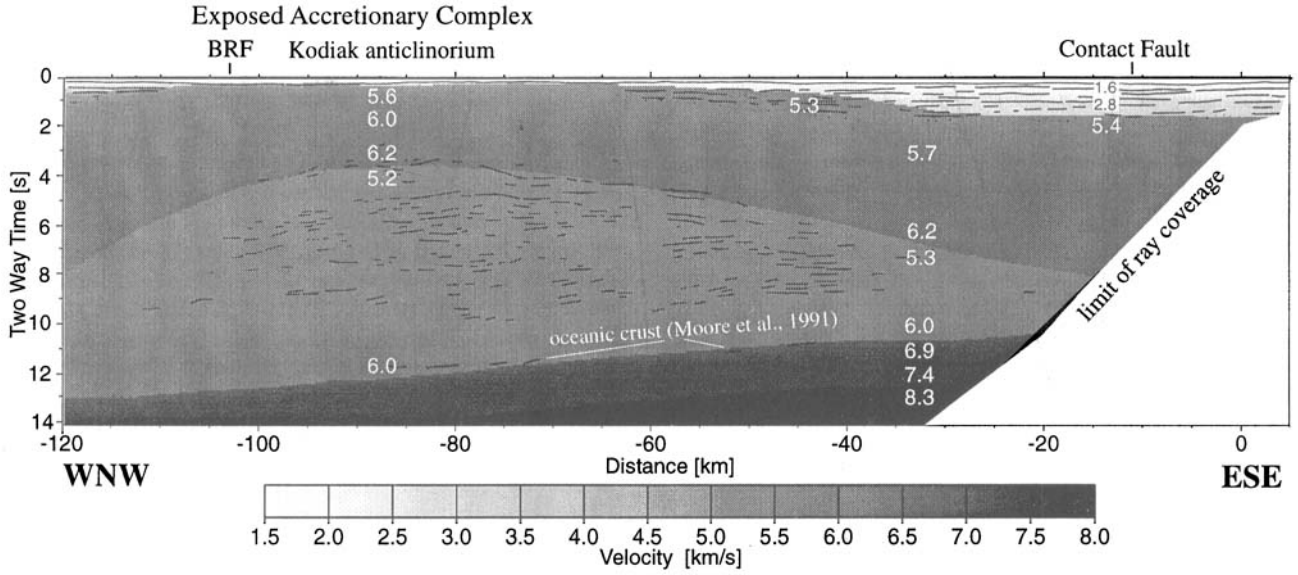

Figure 16. Crustal model with depth converted in two-way time superimposed on line drawings of the reflection data along EDGE 301 (after Moore *et al.* 1991).

same magnitude (> 10 km) (Sample & Moore 1987). The maximum thickness of 23 km of the low-velocity rocks may suggest an even greater uplift along the Kodiak Island–Kenai Peninsula axis and implies concurrent deepening of the subducting oceanic plate due to isostatic compensation.

The low average velocity of the arched reflectors and the large velocity contrast of probably over 1.0 km s^{-1} with the overlying structure is in agreement with the low-velocity rocks in the lower crust beneath the Chugach mountains (Flueh *et al.* 1989; Fuis *et al.* 1991). However, the velocities found there are significantly higher, 6.2–6.5 km s^{-1}, and were interpreted as underplated terranes attached to the subducted oceanic crust (Fuis *et al.* 1991; Brocher *et al.* 1994). Similarly, we regard the large regional-scale extent of these low-velocity rocks beneath the Kodiak shelf as further evidence for the underplating hypothesis proposed by Byrne (1986) and Moore *et al.* (1991). However, a 2-D material balance raises doubt that the underplated rocks are just subducted thick sedimentary sequences.

From the composite crustal section along the EDGE transect (Fig. 17) it is apparent that the cross-sectional area of the underplated body (2090 km^2) is roughly equal to the area interpreted as accreted Eocene and younger rocks (seawards from the vertical wavy line, 2140 km^2). According to Byrne (1986) and Moore *et al.* (1991), the underplating occurred to maintain a stable taper in response to the rapid lateral growth of the accretionary wedge during Eocene and Oligocene times. This equality in turn suggests that the continental growth can be roughly partitioned into frontal accretion and underplating. Assuming the current plate setting (convergence rate 54 km Myr^{-1}, sediment thickness 2 km at the trench) has been sustained since the Eocene, it would require 49 Myr to construct the current continental margin, here additionally taking into account the 20 per cent decrease in volume of the sediment due to the porosity reduction (Frühn 1995). This estimate is a minimum because sediment is subducted and returned to the mantle, and such thick sediment at the trench is a Pleistocene phenomenon (von Huene *et al.* 1987). We conclude that the rapid continental growth in Eocene and Pliocene times requires a high rate of plate convergence and/or an exceptionally thick sedimentary cover on the converging oceanic crust, similar to that along the Makran continental margin in the Gulf of Oman (White & Louden 1982; Platt *et al.* 1985). Alternatively, the underplating of the thick sedimentary sequence may not be the only process responsible for the arched reflectors. We speculate that terranes, a small continental fragment or seamounts and/or seamount chains, even plateau, may contribute to the underplating. However, in order to explain the basic features of the underplated rocks, namely the layered reflectors and the low average velocities, only the seamounts and/or oceanic plateaus are eligible. Investigations across the Hawaii Islands and Quepos Plateau off Costa Rica showed that the seamounts indeed show layered reflections and low velocities (3.7–5.7 km s^{-1}) (Watts *et al.*

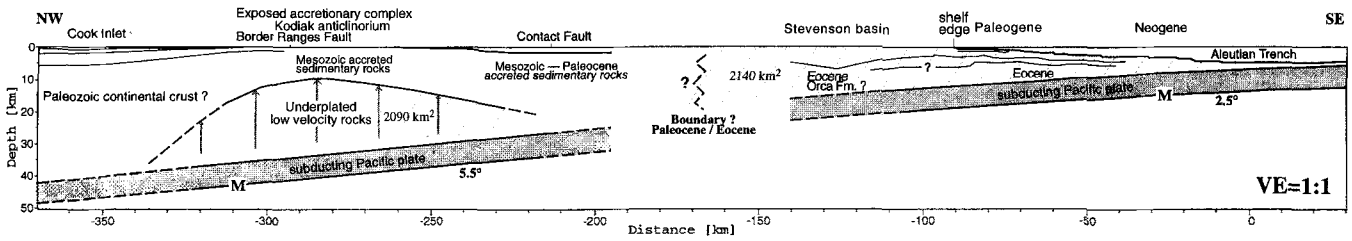

Figure 17. Interpretative sketch of the crustal model along the EDGE transect. The numbers are the sizes of the individual cross-sectional areas (grey hatched), representing the continental growth contributed by the large-scale underplating and the frontal accretion since Eocene times.

1985; Lindwall 1988; Watts & ten Brink 1989; Flores-Hernández 1996). Although it is unclear how the velocities of such rocks change during subduction, the broad spectrum of velocity variation (5.3–6.5 km s^{-1}) of basalts at 20 km depth (Christensen & Mooney 1995) may lend support to the assumption that the velocities of the basalts increase only moderately during the subduction and match the low velocities for the underplated rocks. In addition the velocity increase may depend critically on the fluids trapped during subduction.

CONCLUSION

The crustal structure of the Kodiak Shelf is well resolved by the seismic refraction measurements. These data clearly define a gently dipping Pacific Plate that subducts at the trench at about 2.5° and increases gradually to 5° beneath the inner shelf 250 km landwards of the trench (Fig. 17). This gentle dip is also in good agreement with earthquake and tomographic studies (Kissling & Lahr 1989; Stephens *et al.* 1990; Page *et al.* 1991), which indicate a low-angle subduction zone that steepens abruptly beneath the Cook Inlet. In contrast, along the TACT line the Pacific plate dips with a much larger angle of 10° and flattens abruptly 150 km landwards of the trench axis (Brocher *et al.* 1994). This significant difference in crustal configuration is probably related to the subduction of the Yakutat terrane (Bruns 1983; Brocher *et al.* 1994).

The oceanic crust has a normal velocity–depth function. A rapid increase in the velocity at the top of layer 2 during the subduction has clearly contributed to the reduction in porosity. The velocity at the top of layer 3 increases slowly from the trench.

Below the continental slope the young Neogene accretionary prism occupies the seaward half and is characterized by smooth velocity–depth functions with a large downward- and landward-positive gradient. More consolidated, possibly late Eocene sediment with elevated velocities further landwards acts as a backstop.

A structural break occurs at the shelf edge. The reflection data failed to image the deeper structure seawards of the Stevenson basin. The top of the low-velocity zone can be correlated to the overpressure measured in the nearby borehole. It is unclear, however, if this overpressure persists at depth and is at least partly responsible for the unusually low velocity of about 3.6 km s^{-1} at 6–7 km depth. Since this body lies beneath horizon C, and is therefore older than the late Eocene, a higher velocity is expected. The low velocities beneath the outer shelf are unexplained.

Across the inner shelf between Kodiak Island and Kenai Peninsula, high velocities of over 6.0 km s^{-1} at near-surface levels document strong uplift of the Mesozoic and Palaeocene accretionary complex, and determine its seaward extent beneath the outer shelf. A series of arched reflectors in the lower crust coincide with low-velocity rocks, providing evidence for large-scale underplating. Despite the uncertainty of the detailed internal velocity structure of the LVZ, a material balance shows that the underplating of underthrust sedimentary sequences alone is not sufficient for the huge volume of underplated rocks. We speculate that underplating of terranes, a small continental fragment, or more likely seamounts or even plateau, may be involved in the continental growth. Regardless of what material has been underplated, the question arises, did the underplating occur in response to the rapid lateral growth of the accretionary wedge or vice versa? We favour the latter in that the large-scale underplating facilitates a rapid lateral growth of continental margin, since even in the case of the underplating of thick sedimentary sequences, a large part of the sediment arriving at the trench is underthrust and eventually underplated.

ACKNOWLEDGMENTS

We are grateful to all the participants of the cruise whose efforts made this study possible. Special thanks go to Captain H. Bruns and his skilful crew of the R/V Sonne. The research permit to work in US waters was provided despite a short-notice application through the special effort of N. Krushensky, US Geological Survey. Comments by T. Brocher and E. Kissling considerably improved an earlier version of this manuscript. This project was supported by the BMBF, Bonn, through grant 03G0096 A.

REFERENCES

Bangs, N.L.B., Westbrook, G.K., Ladd, J.W. & Buhl, P., 1990. Seismic velocities from the Barbados Ridge complex: Indicators of high pore fluid pressures in an accretionary complex, *J. geophys. Res.*, **95,** 8767–8782.

Barker, F, Farmer, G.L., Ayuso, R.A., Plafker, G. & Lull, J.S., 1992. The 50 Ma granodiorite of the eastern Gulf of Alaska: Melting in an accretionary prism in the forearc, *J. geophys. Res.*, **97,** 6757–6778.

Brocher, T.M., Fuis, G.S., Fisher, M.A. Plafker, G., Moses, M.J., Taber, J.J. & Christensen, N.I., 1994. Mapping the megathrust beneath the northern Gulf of Alaska using wide-angle seismic data, *J. geophys. Res.*, **99,** 11 663–11 685.

Bruns, T.R., 1983. Model for the origin of the Yakutat Block, an accreting terrane in the northern Gulf of Alaska, *Geology,* **11,** 718–721.

Byrne, T., 1986. Eocene underplating along the Kodiak Shelf, Alaska: Implications and regional correlations, *Tectonics,* **5,** 403–421.

Byrne, T. & Fisher, D., 1987. Episodic growth of the Kodiak convergent margin, *Nature,* **325,** 338–341.

Christensen, N.I., 1978. Ophiolite, seismic velocities, and ocean crustal structure, *Tectonophysics,* **47,** 131–157.

Christensen, N.I. & Mooney, W.D., 1995. Seismic velocity structure and composition of the continental crust: A global view, *J. geophys. Res.*, **100,** 9761–9788.

DeMets, C., Gordon, R.G., Argus, D.F. & Stein, S., 1990. Current plate motions, *Geophys. J. Int.*, **101,** 425–478.

Fisher, M.A., 1980. Petroleum geology of the Kodiak Shelf, Alaska, *Am. Assoc. Petrol. Geol. Bull.*, **64,** 1140–1157.

Fisher, M.A. & Magoon, L.B., 1978. Framework geology of lower Cook Inlet, Alaska, *Am. Assoc. Petrol. Geol. Bull.*, **62,** 373–402.

Fisher, M.A. & von Huene, R., 1984. Geophysical investigation of a suture zone: The Border Ranges fault of southern Alaska, *J. geophys. Res.*, **89,** 11 333–11 351.

Fisher, M.A., von Huene, R., Smith, G.L. & Bruns, T.R., 1983. Possible seismic reflections from the downgoing Pacific Plate, 275 kilometers arcward from the eastern Aleutian trench, *J. geophys. Res.*, **88,** 5835–5849.

Fisher, M.A., von Huene, R. & Smith, G.L., 1987. Reflections from midcrustal rocks within the Mesozoic subduction complex near the eastern Aleutian trench, *J. geophys. Res.*, **92,** 7907–7915.

Flores-Hernández, 1996. Processing and interpretation of multichannel seismic reflection data on continental and oceanic crust of the Pacific margin off Costa Rica, *Diploma thesis,* GEOMAR, University Kiel, Germany.

Flueh, E.R. & Bialas, J., 1996. A digital, high data capacity ocean

bottom recorder for seismic investigations, *Int. Underwater Systems Design,* **18,** 18–20.

Flueh, E.R. & von Huene, R., 1994. FS SONNE, Cruise Report SO96, KODIAK-SEIS, Hong Kong-Kodiak-Kodiak, 09.06.–26.07. 1994, *GEOMAR internal report,* Kiel.

Flueh, E.R., Mooney, W., Fuis, G.S. & Ambos, E., 1989. Crustal structure of the Chugach Mountains, southern Alaska: A study of peg-leg multiples from a low-velocity zone, *J. geophys. Res.,* **94 (B11),** 16 023–16 035.

Frühn, J., 1995. Tektonik und Entwässerung des aktiven Kontinentalrands vor Kodiak Island, Alaska, *PhD thesis,* University Kiel, *GEOMAR Report 39,* Kiel, Germany.

Fuis, G.S., Ambos, E.L., Mooney, W., Christensen, N.I. & Geist, E., 1991. Crustal structure of accreted terranes in southern Alaska, Chugach Mountains and Copper River Basin, from seismic refraction results, *J. geophys. Res.,* **96,** 4187–4227.

Griscom, A. & Sauer, P.E., 1990. Interpretation of magnetic maps of the northern Gulf of Alaska, with emphasis on the source of the Slope anomly, *USGS Open File Rept,* 90–348.

Hill, M.D., Morris, J. & Whelan, J., 1981. Hybrid granodiorites intruding the accretionary prism, Kodiak, Schumagin and Sanak Islands, southwest Alaska, *J. geophys. Res.,* **86,** 10 569–10 590.

Hwang, L.J. & Mooney, W.D., 1986. Velocity and Q structure of the great valley, California, based on synthetic seismogram modeling of seismic refraction data, *Bull. seism. Soc. Am.,* **76,** 1053–1067.

Jones, D.L., 1982. Preliminary tectonographic terrane map of the Circum-Pacific region, *Am. Assoc. Petrol. Geol. Bull.,* **66,** 972–982.

Kissling, E. & Lahr, J.C., 1989. Tomographic image of the Pacific slab under southern Alaska, *Eclogae Geol. Helv.,* **84,** 297–315.

Lindwall, D.A., 1988. A two-dimensional seismic investigation of crustal structure under the Hawaii Islands near Oahu and Kauai, *J. geophys. Res.,* **93,** 12 107–12 122.

Luetgert, J., 1992. MacRay – Interactive two-dimensional seismic raytracing for the Macintosh, *USGS Open File Rept,* 92–356, Menlo Park, CA.

Moore, J.C., Byrne, T., Plumley, P.W., Reid, M., Gibbons, H. & Coe, R.S., 1983. Paleogene evolution of the Kodiak islands, Alaska: Consequences of ridge-trench in a more southerly latitude, *Tectonics,* **2,** 265–293.

Moore, J.C. *et al.,* 1991. EDGE deep seismic reflection transect of the eastern Aleutian arc-trench layered lower crust reveals underplating and continental growth, *Geology,* **19,** 420–424.

Page, R.A., Biswas, N.N., Lahr, J.C. & Pulpan, H., 1991. Seismicity of continental Alaska, in *Neotectonics of North America: Decade Map,* Vol. 1, pp. 47–68, eds Slemmons, D.B., Engdahl, E.R., Zoback M.D. & Blackwell, D.D., Geol. Soc. Am., Boulder, CO.

Plafker, G., Nokleberg, W.J. & Lull, J.S., 1989. Bedrock geology and tectonic evolution of the Wrangellia, Peninsular, and Chugach terranes along the Trans-Alaska Crustal Transect in the Chugach Mountains and southern Copper River basin, Alaska, *J. geophys. Res.,* **94,** 4255–4295.

Plafker, G., Moore J.C. & Winkler, G.R., 1994. Geology of the southern Alaska margin, in *The Geology of North America, G-1, The Geology of Alaska,* pp. 389–449, eds Plafker, G. & Berg, H.C., Geol. Soc. Am., Boulder, CO.

Platt, J.P., Leggett, J.K., Young, J., Raza, H. & Alam, S., 1985. Large-scale sediment underplating in the Makran accretionary prism, southwest Pakistan, *Geology,* **13,** 507–511.

Salisbury, M.H. & Christensen, N.I., 1978. The seismic velocity structure of a traverse through the Bay of Islands ophiolite complex, Newfoundland, An exposure of oceanic crust and upper mantle, *J. geophys. Res.,* **83,** 805–817.

Sample, J.C & Moore, J.C., 1987. Structural style and kinematics of an underplated slate belt, Kodiak and adjacent islands, Alaska. *Geol. Soc. Am. Bull.,* **99,** 7–20.

Shipley, T.H. & Moore, G.F., 1986. Sediment accretion, subduction and dewatering at the base of the trench slope off Costa Rica, *J. geophys. Res.,* **91,** 2019–2028.

Shipley, T.H., Stoffa, P.L. & Dean, D.F., 1990. Underthrust sediments, fluid migration paths, and mud volcanoes associated with the accretionary wedge off Costa Rica: Middle American Trench, *J. geophys. Res.,* **95,** 8743–8752.

Spudich, P. & Orcutt, J., 1980a. Petrology and porosity of an oceanic crustal site: results from wave form modeling of seismic refraction data, *J. geophys. Res.,* **88,** 1409–1433.

Spudich, P. & Orcutt, J., 1980b. A new look of at the seismic structure of the oceanic crust, *Rev. Geophys.,* **88,** 1409–1433.

Stephens, C.D., Page, R.A. & Lahr, J.C., 1990. Reflected and mode-converted seismic waves within the shallow Aleutian subduction zone, southern Kenai Peninsula, Alaska, *J. geophys. Res.,* **95,** 6883–6897.

Stevenson, A.J. & Embley, R., 1987. Deep-sea fan bodies, terrigenous turbidite sedimentation, and petroleum geology, Gulf of Alaska, in *Geology and Resource Potential of the Continental Margin of Western North America and Adjacent Ocean Basins – Beaufordsea to Baja California,* eds Scholl, D.W., Grantz, A. & Vedder, J.G., Circum-Pacific Council for Energy and Mineral Resources, *Earth Science Series,* **6,** 503–522, Houston, TX.

Suess, E., 1994. FS SONNE Cruise Report SO97, KODIAK-Vent, Kodiak-Dutch Harbour-Tokyo-Singapore, 27.7.–19.9. 1994, *GEOMAR Report,* **29,** Kiel.

Turner, R.F. *et al.,* 1987. *Geological and operational summary, Kodiak Shelf Stratigraphic Test Wells, Alaska,* US Department of Interior Minerals Management Service OCS Report, MMS 87–0109.

von Huene, R., Fisher, M.A. & Bruns, T.R., 1987. Geology and Evolution of the Kodiak Margin, Gulf of Alaska, in *Geology and Resources of Western North America,* Vol. 6, pp. 191–212, eds Scholl, D.W., Grantz, A. & Vedder, J.G., Houston, TX.

von Huene, R., Klaeschen, D., Gutscher, M.A. & Frühn, J., 1997. Mass and fluid flux during accretion at the Aleutian margin, *Geol. Soc. Am. Bull.,* submitted.

Watts, A.B. & ten Brink, U.S., 1989. Crustal structure, flexure and subsidence history of the Hawaiian Islands, *J. geophys. Res.,* **94,** 10 473–10 500.

Watts, A.B., ten Brink, U.S., Buhl, P. & Brocher, T.M., 1985. A multichannel seismic study of lithospheric flexure across the Hawaii-Emperor seamount chain, *Nature,* **315,** 105–111.

White, R.S. & Louden, K.E., 1982. The Makran continental margin: Structure of a thickly sedimented convergent plate boundary, in *Studies in Continental Margin Geology,* eds Watkins, J.S. & Drake C.L., *Am. Assoc. Petrol. Geol. Mem.,* **34,** 499–517.

White, R.S., McKenzie, D. & O'Nions, R.K., 1992. Oceanic crustal thickness from seismic measurements and rare earth element inversions, *J. geophys. Res.,* **97,** 19 681–19 715.

Zelt, C.A. & Smith, R.B., 1992. Seismic traveltime inversion for 2-D crustal velocity structure, *Geophys. J. Int.,* **108,** 16–34.